Author's Summary of the Dissertation

for the award of the educational and scientific degree "Doctor" in the field of higher education 4. "Natural Sciences, Mathematics and Informatics"

Professional field: code 4.3 "Biological Sciences"
Scientific specialty "Biophysics"

on the topic of:

Antitumor lipids – effects on transmembrane cellular signalling

Tihomira Tihomirova Stoyanova

Scientific supervisors: Prof. Dr Rumiana Tzoneva

Prof. Dr Albena Momchilova, DSc

Laboratory "Transmembrane Signaling"

2026

The dissertation comprises 128 pages and includes 26 figures and 3 tables. The bibliography contains 236 references. The results achieved have been published in three scientific papers. The dissertation was presented and discussed at an extended seminar of the Institute of Biophysics and Biomedical Engineering, Bulgarian Academy of Sciences, held on 05.12.2025.

Съдържание:

Abbreviations

7AA-D - 7-aminoactinomycin D
ACF - autocorrelation function
AO - acridine orange
BNCs - binucleated cells
CBMN - cytokinesis-block micronucleus assay
CDK- cyclin-dependent kinase
CHEK1- checkpoint Kinase 1
Chol - cholesterol
CI- combination index
DAPI - 4',6-diamidino-2-phenylindole
DMS - D-erythro-N,N-dimethylsphingosine
DMSO - dimethyl sulfoxide
EGFR - epidermal growth factor receptor
EPC3 - erufosine; erucylphospho-N,N,N-trimethylpropanolamine
EtBr - ethidium bromide
FPV-HA - influenza A virus hemagglutinin
GaAsP - gallium arsenide phosphide detector
GFP - green fluorescent protein
GP - general polarization
HA - hemagglutinin
hEGFR - human epidermal growth factor receptor
HePC- miltefosine
JNK1 - c-Jun N-terminal Kinase 1
mit-C - mitomycin C
MN - micronuclei
mTOR - mechanistic target of rapamycin
NB - nuclear buds
NPB - nucleoplasmic bridges
PC – phosphatidylcholine
PE - phosphatidylethanolamine
PFA – paraformaldehyde
PI - propidium iodide
PI – phosphatidylinositol
PI3K - phosphoinositide 3-kinase
PKCα – protein kinase C α
PKCζ – protein kinase Cζ
PMA – phorbol 12-myristate 13-acetate
PS – phosphatidylserine

S1P - sphingosine-1-phosphate
sFCS - scanning fluorescence correlation microscopy
SK1 - sphingosine kinase 1
SM – sphingomyelin
Sph - sphingosine
TLC - thin-layer chromatography
TRITC - tetramethylrhodamine B isothiocyana

Chapter 1. Introduction

Cancer remains one of the leading causes of premature death and a major obstacle to increasing life expectancy worldwide [Bray F. I. et al., 2021]. In Bulgaria, oncological diseases are the second most common cause of death, with 32,817 new cases reported in 2022, of which 18,794 resulted in death [Sung H. et al., 2021]. Globally, breast cancer is the most common malignancy, followed by lung cancer. In Bulgaria, however, these cancers rank third and second, respectively. Breast cancer remains the primary cause of cancer-related death among women [Sung H. et al., 2021]. Breast tumours are characterised by high biological heterogeneity, a strong tendency to metastasise, and frequent development of therapy resistance. Conventional chemotherapeutic agents currently used are highly toxic and produce notable side effects. These factors highlight the need for new therapeutic strategies that are effective against aggressive breast cancer subtypes, do not induce resistance, and exhibit fewer adverse effects. Accordingly, this dissertation investigates the antitumour effect of the lipid agent erufosine (EPC3). Erufosine is an alkylphosphocholine that acts differently from standard chemotherapeutic agents by targeting the cell membrane, where it modulates multiple signal transduction pathways involved in cell survival and migration. It can be administered intravenously and does not induce resistance [Jimenez-Lopez J. M. et al., 2010; Chometon G. et al., 2014; Dineva I. et al., 2012]. The dissertation includes experiments aimed at evaluating its potential application in treating one of the most challenging tumour subtypes—triple-negative breast cancer. In addition

to erufosine, the antitumour effect of another alkylphosphocholine, miltefosine (HePC), is also investigated in this study. Miltefosine is used in the treatment of leishmaniasis and Chagas disease [Kuhlencord A. et al., 1992; Pachioni-Vasconcelos J. A. et al., 2016]. It possesses anti-inflammatory, antibacterial, fungicidal, and antitumour properties [Park S.-Y. et al., 2021]. HePC affects multiple signal transduction pathways that regulate cell survival and migration [Valenzuela-Oses J. K. et al., 2017; Park S.-Y. et al., 2021]. Miltefosine inhibits CHEK1, leading to cell cycle arrest at the G2/M phase and inducing cell death independently of p53 status, thereby significantly broadening the range of tumour types to which it may be applied [Park S.-Y. et al., 2021]. Nonetheless, its clinical application is limited due to its high toxicity and side effects. To reduce therapeutic doses and enhance its antitumour effect, this study explores the potential of miltefosine in combination with D-erythro-N,N-dimethylsphingosine (DMS). DMS is a sphingolipid with anti-inflammatory, antiparasitic, and antitumour properties [Vasconcelos J. F. et al., 2017]. It modulates the so-called “sphingolipid rheostat,” which plays a key role in controlling cell survival and death [Herr D. R. and Chun J., 2007]. Furthermore, DMS enhances tumour cells' sensitivity to conventional chemotherapeutic agents [Shida D. et al., 2008; Igarashi Y. et al., 1990]. These characteristics suggest that combining these two lipids may yield a synergistic antitumour effect and pave the way for developing a novel therapeutic approach. Consequently, this research investigates the effects of these two antitumour lipids in the context of developing combination therapy for lung cancer, which is the leading cause of cancer-related mortality among men [Sung H. et al., 2021].

This dissertation aims to contribute to the development of a new class of lipid-based therapies characterised by low toxicity and high efficacy in treating breast and lung cancers—two malignancies with significant global and national health and societal impacts.

Chapter 2. Aim and Objectives

The aim of this dissertation is to explore how antitumor lipids affect transmembrane signalling in cancer cells.

To accomplish the objectives of the dissertation, the following tasks were established:

1. Performing a cytotoxicity analysis of the effects of EPC3, DMS, and HePC (administered individually and in combination) on cancer cells with varying levels of invasiveness.
2. 2. Examining the type of cell death induced following treatment with the antitumour lipids (individually and collectively).
3. 3. Quantitative assessment of the resulting cell death.
4. 4. Exploring the effects of the antitumour lipids on the cell cycle, cell migration, cellular morphology, and the cytoskeleton.
5. 5. Studying the influence of the antitumour lipids on membrane fluidity and the diffusion dynamics of the cell membrane.
6. 6. Analysing the impact of the antitumour lipids on the sphingolipid rheostat.

Chapter 3. Materials and Methods

I. Materials

1. Antitumor agents

In the present dissertation, three antitumor agents were used to treat cancer and normal (control) cells: erufosine, miltefosine, and DMS.

2. Reagents

2.1. Reagents used for the assessment of cell viability and cell death

• MTT reagent (Invitrogen, Germany)

• Acridine Orange (Sigma-Aldrich, Germany)

• Ethidium bromide (Sigma-Aldrich, Germany)

• Annexin V Apoptosis Detection Kit FITC (Affymetrix, eBioscience, Austria)

2.2. Reagents used for preparing microscopic samples

• Phalloidin/Tetramethylrhodamine B isothiocyanate (TRITC) (Sigma-Aldrich, Germany)

• 4′,6-diamidino-2-phenylindole dihydrochloride (DAPI) (Sigma-Aldrich, Germany)

• Di-4-ANEPPDHQ (Molecular Probes, Eugene, OR, USA)

• Plasmid encoding the Epidermal Growth Factor Receptor (EGFR) fused with Enhanced Green Fluorescent Protein (EGFP) (hEGFR-EGFP), kindly provided by Alexander Sorkin (Addgene plasmid #32751)

• Plasmid encoding the haemagglutinin (HA) gene from influenza virus strain A/FPV/Rostock/34 (H7N1), tagged at the C-terminus with monomeric EGFP (mEGFP) (FPV-HA-mEGFP) (Addgene #127810)

2.3. Reagents used for immunological analyses

• ELISA kit for detecting human Sphingosine-1-phosphate (S1P) (Antibody Research Corporation, USA)

• Reagents used for analysing PKC phosphorylation levels:

• anti-phosphorylated PKCα (p-PKCα) antibody (Santa Cruz Biotechnology)

• antibody specific for total PKCα (Santa Cruz Biotechnology)

• HRP-conjugated secondary antibodies (Enzo Life Sciences)

• Western Blotting Luminol Reagent (Santa Cruz) and Kodak X-ray film for immunoblot visualisation

2.4. Reagents used for enzyme activity assays

• Cytochrome C Reductase (NADPH) Assay Kit (Sigma-Aldrich, Germany)

3. Cell lines

• Breast cancer cell lines: MCF-7 and MDA-MB-231

• Mammary epithelial cell line: MCF-10A

• Human non-small cell lung carcinoma cell line: A5499

- Human umbilical vein endothelial cell line: HUVEC

All cell lines used as in vitro model systems were purchased from ATCC (Manassas, VA, USA).

II. Methods

1. MTT assay

The MTT assay was employed to assess cell viability after treatment with antitumour agents. The method relies on the formation of formazan crystals, which are then dissolved in acidified isopropanol, and the resulting colour intensity is measured quantitatively using a spectrophotometer. Absorbance was recorded at $\lambda = 570$ nm with a microplate reader (Tecan Infinite F200 PRO, Tecan Austria GmbH, Salzburg). The colourimetric intensity of the reaction product correlates with the viability of the cells in the sample.

2. Vital staining with AO/EtBr

This method was employed to analyse the type of cell death induced by antitumour agents. Acridine orange (AO) is a vital dye that fluoresces green (525 nm) when bound to DNA and red (650 nm) when attached to RNA. Ethidium bromide (EtBr) intercalates between DNA strands and penetrates only cells with compromised membrane integrity. When bound to DNA, its emission maximum occurs in the orange spectral region (590 nm). The resulting staining offers information on the type of cell death induced by antitumour treatment. Microscopic images were captured using a fluorescence microscope NU-2, Carl Zeiss, Germany, equipped with a Canon EOS 5D Mark II camera and a 25× objective.

3. In Vitro cell migration assay (Scratch Assay)

A wound-healing assay was used to assess the effects of antitumour agents on tumour cell migration. Wound closure was observed by capturing images of each well with a Leica DMI300B microscope (Leica

Microsystems, Germany). Images were analysed using ImageJ software. Statistical analysis was conducted with GraphPad Prism 5.02. The percentage of wound closure was determined by normalising the difference in area relative to the initial wound area at T_0.

4. Cell morphology

Phase-contrast microscopy of live cells was carried out to assess the impact of antitumour agents on cell morphology. Images were captured using an inverted phase-contrast microscope (MEIJI, Japan) with a 20× objective (Phase DM, MEIJI, Japan) and an Optikam B1 Digital camera (Optica, Italy).).

5. DAPI staining

The effect of antitumor agents on nuclear structure was examined. For this purpose, cells were stained with 1 μg/mL DAPI following fixation with 3% paraformaldehyde (PFA). Fluorescent nuclei were observed using a fluorescence microscope (Jenalumar, Carl Zeiss, Germany) with a 100× objective. Apoptotic cells were identified based on nuclear condensation and fragmentation.

6. Flow cytometric analysis of apoptosis and necrosis

Quantitative analysis of cell death was performed using the Annexin V Apoptosis Detection Kit FITC. The binding of Annexin V/FITC to phosphatidylserine (PS) indicates the initiation of apoptosis and is characterised by an emission maximum at 518 nm. 7-AAD binds double-stranded DNA and does not penetrate intact cell membranes; therefore, its presence indicates necrotic changes. The emission maximum of 7-AAD is 647 nm, allowing discrimination between the two dyes and the

determination of cell death type. Samples were analysed using a BD FACSCalibur flow cytometer, and data were processed using FlowJo v10.1 software.

7. Nicoletti flow cytometric assay for cell cycle analysis

To determine the percentage distribution of cells in different phases of the cell cycle following treatment with antitumor agents, flow cytometric analysis was performed using the Nicoletti method, which stains DNA with propidium iodide. Cell cycle phase distribution was determined based on DNA content. Samples were analysed using a BD FACSCalibur flow cytometer and FlowJo v10.1 software.

8. Determination of mRNA levels by RT-PCR

Total RNA isolated using TRIzol reagent was reverse-transcribed into cDNA using SuperScript™ II reverse transcriptase, a modified version of MMLV reverse transcriptase with increased thermostability and reduced RNase H activity. RNA quantity was determined using a NanoDrop spectrophotometer. Gene-specific primers and TaqMan probes were designed using Primer Express® Software v3.0.1. RT - qPCR was performed using a real-time PCR system - Rotor-Gene 6000.

9. Analysis of cell adhesion by phalloidin-TRITC staining

The effects of antitumor agents on the adhesive properties of cancer cells were examined by fluorescent staining with phalloidin-TRITC and DAPI nuclear staining. Samples were analysed using an Axiovert 200 M fluorescence microscope (Plan-Apochromat 63×/1.40 Oil DIC M27 objective; AxioCam MR3 camera), followed by image processing in ImageJ.

10. Confocal microscopy using Di-4-ANEPPDHQ

To investigate the effect of antitumor agents on plasma membrane fluidity in cancer cells, confocal microscopy was performed using the polarity-sensitive fluorescent probe Di-4-ANEPPDHQ. Images were acquired with a Zeiss LSM 780 confocal microscope (Carl Zeiss, Oberkochen, Germany) and a pixel size of 200 nm (512 × 512 pixels) using a Plan-Apochromat 40×/1.2 Korr DIC M27 water-immersion objective. Excitation was performed using a 488 nm argon laser. Fluorescence was detected between 498–579 nm (Channel 1) and 620–750 nm (Channel 2) after passing through a 488 nm dichroic mirror, using a gallium arsenide phosphide (GaAsP) detector. Out-of-focus fluorescence was reduced using a 42.4 μm pinhole. Data were presented as normalised histograms of selected pixels.

11. Lipid extraction and phospholipid analysis

Cells were treated with various concentrations of EPC3 for 24 h and subjected to total lipid extraction using a chloroform:methanol:water system in amounts predetermined according to the chloroform–methanol–water phase diagram *[Bligh E.G.and Dyer W.J, 1959; Pankov R. et al.,2006]*. Lipid extracts were concentrated using a vacuum evaporator. Individual phospholipid fractions were separated on silica gel G60 TLC plates (20 × 20 cm, Merck, Darmstadt, Germany). Fractions were visualised by iodine staining, scraped, and quantified by inorganic phosphorus determination *[Kahovcova J. and Odavic, R., 1969]*.

12. Determination of cholesterol content by gas chromatography

Cholesterol content in membranes of cancer cells treated with IC_{50} and IC_{75} concentrations of EPC3 was determined by gas chromatography *[Nikolova-Karakashian M.N. et al. 1992]* using a Carlo-Erba gas chromatograph equipped with a flame ionisation detector. Chromatographic separation was performed isothermally at 190 °C using a 2 m column coated with 10% diethylene glycol succinate (DEGS) on Chromosorb W 60/80 mesh (Pharmacia Fine Chemicals Inc., Piscataway, NJ, USA). Nitrogen was used as the carrier gas in conditions which provide optimal resolution and reproducibility. Quantification was performed using external standard curves, and cholesterol peaks were identified based on retention time and spectral characteristics.

13. Scanning fluorescence correlation spectroscopy (sFCS) of cells

Cancer cells treated with EPC3 were transfected with 200 ng (mp-mEGFP or mp-mEGFP(2×)) or 600 ng (hEGFR-EGFP or A/FPV-HA-mEGFP) plasmid DNA using Lipofectamine™ 3000 according to the manufacturer's instructions (Thermo Fisher Scientific, Waltham, MA, USA). After additional 24 h incubation, scanning fluorescence correlation spectroscopy (sFCS) was performed using a Zeiss LSM 780 microscope with a Plan-Apochromat 40×/1.2 Korr DIC M27 water-immersion objective. Samples were excited with a 488 nm argon laser, and fluorescence was detected between 499–597 nm using a GaAsP detector. Membranes were linearly scanned with 256 × 1 pixels (80 nm pixel size) perpendicular to the membrane (crossing the membrane), with

a scan time of 403.20 μs. The total scanning time for each experiment is 3 min. Images (TIFF files) were analyzed using MATLAB with custom-written code. Statistical analysis was performed using one-way ANOVA test, followed by Bonferroni's multiple comparisons test. Differences were considered significant at $p < 0.01$.

14. Immunoblot analysis for determination of PKCα phosphorylation level in cells

Changes in PKCα phosphorylation appeared following cancer cells treatment with antitumor agent were analyzed by Western blotting. Quantitative analysis of signal intensity was performed using ImageJ software. p - PKCα levels were normalized to the signal representing total PKCα and expressed as a percentage of p – PKCα expression in control cells.

15. Cytokinesis-Block Micronucleus Assay (CBMN) on Cells

The CBMN assay was performed according to Fenech et al. *[Fenech M. et al., 2007]* with modifications adapted to the experimental design. Tumor cells were treated with antitumor agents alone or in combination. Mitomycin C (mit – C) was used as a positive control. After 24 h treatment, the medium of each well was replaced with medium containing Cytochalasin B (cyt – B) with a final concentration of 4 μg/mL. Giemsa staining was used for differential visualization of cytoplasm and nuclei. CBMN biomarkers were scored at 1000× magnification of optical microscope (Jena Lumar, Germany). A total of 500 binucleated cells (BNCs) per sample were analyzed to determine the

frequency of micronuclei (MN), nucleoplasmic bridges (NPB), and nuclear buds (NB). Experiments were performed in triplicate.

16. ELISA assay for sphingosine-1-phosphate determination in cells

The effect of single or combined drug treatments on sphingosine-1-phosphate (S1P) levels in cancer cells was determined using a sandwich ELISA kit (Cat. #682861, Antibody Research Corporation, USA). Absorbance was measured using a microplate reader (Tecan Austria GmbH, Salzburg). S1P concentrations in the samples were calculated based on color intensity.

17. Cytochrome C reductase (NADPH) assay

The level of changes in cytochrome C reductase activity following treatment with antitumor agents were assessed using a Cytochrome c Reductase (NADPH) Assay Kit (Cat. # CY0100, Sigma-Aldrich, Germany). The samples were prepared according to manufacturer's recommendations. Optical density was measured at 550 nm using a UV/Vis spectrophotometer (Specord 210 PLUS, Germany). Software WinAspect with kinetic program was used. Enzyme activity was expressed in units/mL.

18. Calculation of the combination index (CI)

The effect of combining two or more agents was evaluated using the combination index (CI) *[Zhao L. et al., 2004]*. CI values were calculated using the data of MTT assay of cells treated with single agent or combination. The calculation of CI was performed using the following formula:

$$CI = [Ca,x/ICx,a] + [Cb,x/ICx,b]$$

Where Ca,x and Cb,x are the concentrations of agent A and B used for treatment to achieve an x% effect. ICx,a and ICx,b are the concentrations of single agents used to chieve the same effect *[Zhao L. et al., 2004]*. A synergistic effect is observed upon treatment with the combination of the two agents when $CI < 1$, whereas an antagonistic effect is observed when $CI > 1$

Chapter 4. Results and Discussion

Part I. Investigation of the effect of erufosine on breast cancer cell lines with different metastatic potential

In the first part, the results of experiments performed with two breast cancer cell lines - MCF-7 and MDA-MB-231 are presented, as well as with a non-tumorigenic epithelial cell line from the mammary gland - MCF-10A. The effect of erufosine on cell viability, the cytoskeleton, the type of induced cell death, the cell cycle, the composition and structure of cellular membranes, as well as the mechanical properties of the cell membrane, were investigated.

1. Cell viability after treatment with erufosine

The MTT assay was used to assess the effect of EPC3 on breast cancer cell viability. MDA-MB-231, MCF-7, and MCF-10A cells were treated with EPC3 at concentrations ranging from 2.5 μM to 100 μM. The IC_{50} values of EPC3 at 24, 48, and 72 h were determined and subsequently used for the treatments applied in the remaining experiments of the present dissertation. In comparison with MDA-MB-231 cells (19.79 μM IC_{50} at 24 h), the low-invasive breast cancer cell line MCF-7 exhibited lower sensitivity to EPC3 (49.09 μM IC_{50} at 24 h) (Fig. 1). In both cell lines, inhibition of cell viability increased with increasing concentration and time of treatment and was more pronounced in the highly metastatic MDA-MB-231 cell line. EPC3 did not affect the viability of normal MCF-10A cells at concentrations that inhibited cancer cell viability, consistent with the lack of side effects observed upon *in vivo* application (Fig. 1).

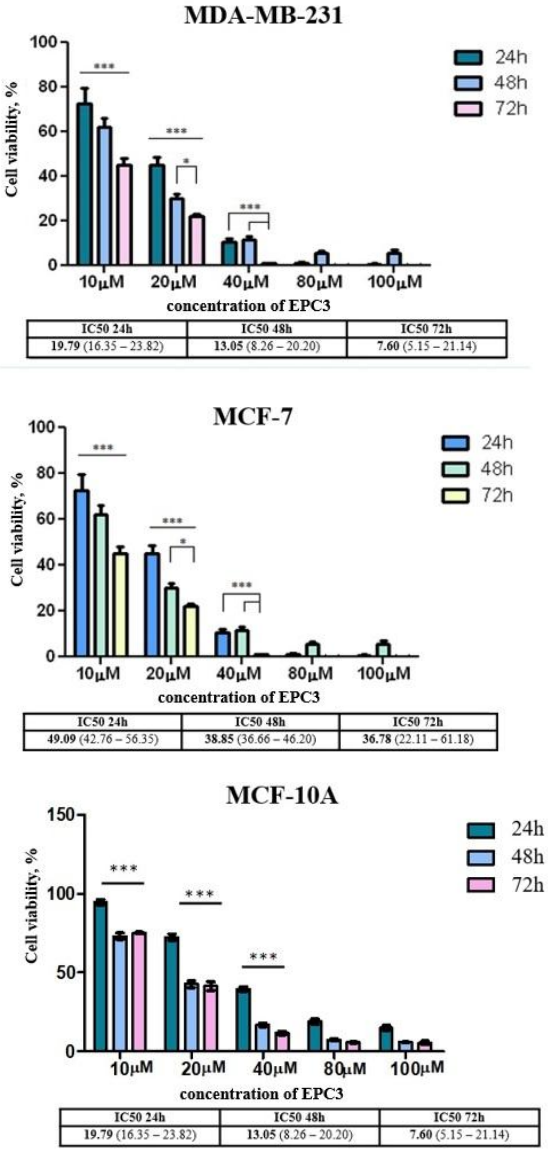

*Fig. 1. Cell viability of MDA-MB-231, MCF-7, and MCF-10A cells treated with erufosine for 24, 48, and 72 h. Statistical analysis was performed using one-way ANOVA, followed by Tukey's post hoc test ($p < 0.05$; *$p < 0.01$; **$p < 0.001$).*

2. Changes in the cell cycle after treatment with erufosine

Flow cytometric analysis according to the Nicoletti method *[Nicoletti I. et al., 1991]* was performed to quantitatively determine the proportion of cells entered process of apoptosis under the influence of erufosine. The analysis was conducted using the breast cancer cell lines MDA-MB-231 and MCF-7, as well as the non-tumorigenic cell line MCF-10A.

Cell cycle analysis of the MCF-7 cell line revealed a time- and dose-dependent increase in the sub-G1 population, which is a characteristic hallmark of apoptosis *[Murad H. et al., 2016]* (Fig. 2A). As early as 24 h after treatment with the IC_{50} of EPC3, the sub-G1 population increased approximately four times compared to control cells, while after 48 h of treatment with the IC_{75}, the proportion of cells in the sub-G1 phase rose to approximately 50% (Fig. 2B). EPC3 also affected the synthetic phase (S phase), manifested by an approximately two times decrease in the S-phase population at 24 and 48 h following treatment with the IC_{50} of EPC3 (Fig. 2A and B).

Upon treatment of the highly invasive MDA-MB-231 cells with erufosine, an increase in the sub-G1 and G2/M cell populations was observed, with both populations increasing in a dose- and time-dependent manner (Fig. 2A and B). In contrast to MCF-7 cells, in which the sub-G1 population predominates, MDA-MB-231 cells exhibit accumulation of a substantial proportion of cells in the G2/M phase (Fig. 2A and B).

With increasing treatment concentration, a further rise in the sub-G1 population was detected, and increasing the dose to IC_{75} resulted in a significant increase in the percentage of cells in this population, reaching up to 6% after 24 h and 17.68% after 48 h. In parallel, treatment with

EPC3 reduced the number of cells in S phase (Fig. 3A and B). Unlike MCF-7 cells, the highly invasive cell line also exhibited an increase in the number of polyploid cells (>4N) (Fig. 3A and B).

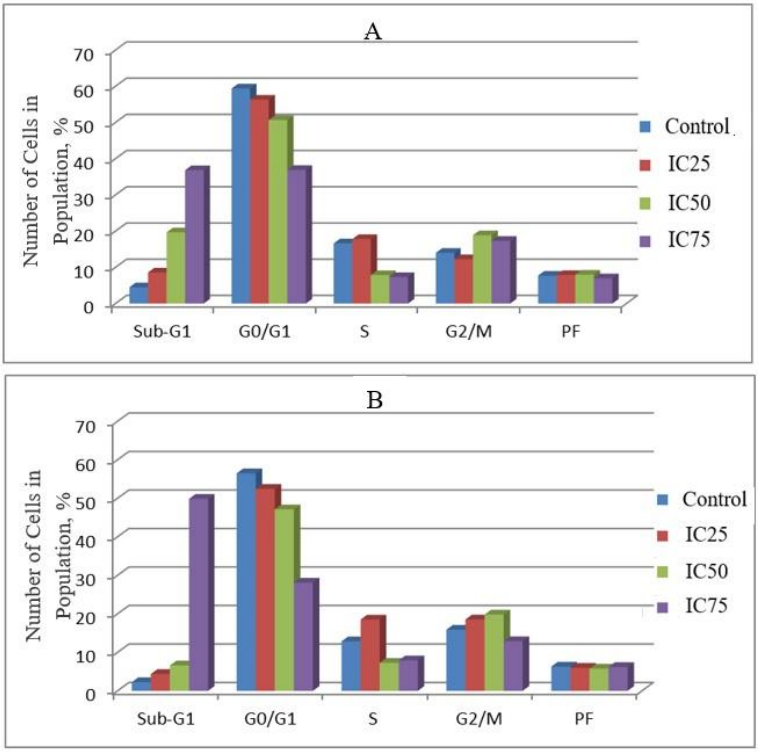

Fig. 2. Flow cytometric analysis of the cell cycle of MCF-7 cells treated with erufosine for 24 h (A) and 48 h (B). The graphs show the distribution of cells in each phase of the cell cycle (Sub-G1, G0/G1, S, and G2/M), as well as the polyploid fraction (PF).

In summary, the observed alterations in the G_2/M and S phases in MDA-MB-231 and MCF-7 cells treated with EPC3 confirm that this antitumor agent disrupts the normal dynamics of the cell cycle.

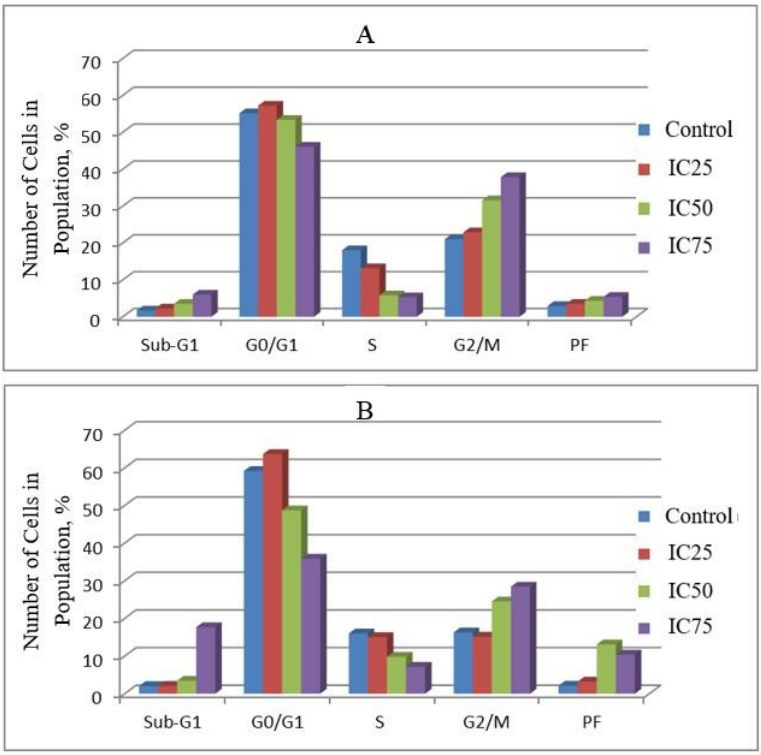

Fig. 3. Flow cytometric analysis of the cell cycle of MDA-MB 231 cells treated with erufosine for 24 h (A) and 48 h (B). The graphs show the distribution of cells across the cell cycle phases (Sub-G1, G0/G1, S, and G2/M) and the polyploid fraction (PF).

There is evidence that erufosine induces cell cycle arrest in leukemic cells by regulating cyclin D1 and cyclin D1-dependent protein kinases *[Kapoor V. et al., 2012]*. Cyclins and cyclin-dependent kinases function together to regulate the cell's transition from one phase of the cell cycle to another *[Hochegger H. et al.,2008]*.

This dissertation studies the effect of EPC3 on the expression of cyclins B and E2, as well as two cyclin-dependent kinases (CDK1 and

CDK2) in MCF-7 and MDA-MB-231 cells (Figs. 4 and 5). Cyclin B and its partner, cyclin-dependent protein kinase CDK1, control the transition of cells from G2 to M-phase, while the pair of E2 and CDK2 regulates the transition from G1 to S-phase of the cell cycle [*Casimiro M.C. et al., 2012*].

The presented results demonstrate that the expression of CDK1 and CDK2 is suppressed in a dose- and time-dependent manner at 24 and 48 h (Fig. 4). At 72 h, however, a recovery of expression levels to values characteristic of the threshold range is observed, with MCF-7 cells even showing a slight increase in CDK1 expression (Fig. 4).

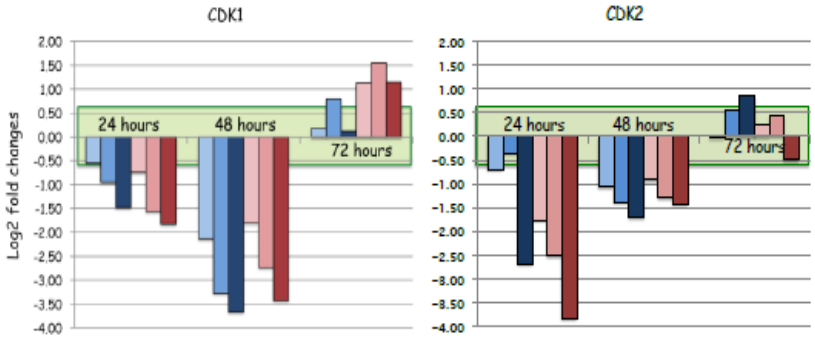

Fig. 4. Graphical representation of RT-qPCR analysis of CDK1 and CDK2 gene expression in MDA-MB-231 (blue) and MCF-7 (pink) cells treated with erufosine for 24, 48, and 72 h. Increasing concentrations of the compound are indicated by increasing intensity of the respective colour. Quantitative differences in gene expression in treated cells relative to controls are presented as log_2 fold changes. The threshold zone for non-significant changes in expression is shown in green and, in the present study, was defined as a 1.5-fold change.

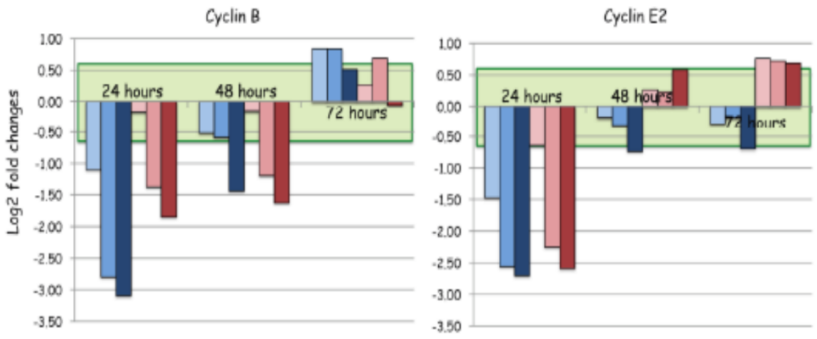

Fig. 5. Graphical representation of RT-qPCR analysis of cyclin B and cyclin E2 gene expression in MDA-MB-231 (blue) and MCF-7 (pink) cells treated with erufosine for 24, 48, and 72 h. Increasing concentrations of the compound are indicated by increasing intensity of the respective colour. Quantitative differences in gene expression in treated cells relative to controls are presented as log_2 fold changes. The threshold zone for non-significant changes in expression is shown in green and, in the present study, was defined as a 1.5-fold change.

A very similar expression profile of the investigated cyclins B and E2 is shown in Fig. 5. A strong dose-dependent suppression of cyclin B expression is observed at 24 and 48 h in both cell lines, whereas at 72 h the expression levels return to the threshold range. The expression of the cyclin E2 gene is significantly reduced at 24 h; however, from 48 h onward, its levels in both cell lines reach normal values.

The decreased expression of CDK2 and cyclin E2, which are responsible for the G1/S transition, explains the increase in the G1 cell population. Conversely, the reduced levels of CDK1 and cyclin B, which govern entry into the M phase and progression through mitosis, may account for the higher proportion of cells in the G2/M phase. The data on erufosine-induced changes in the expression levels of these two cyclins and their associated cyclin-dependent kinases, along with the performed FACS analysis, clearly show that erufosine causes cell cycle arrest in

cancer cells at the G1/S and G2/M checkpoints, with a notably stronger effect on the G2/M transition. Furthermore, the highly invasive MDA-MB-231 cell line was found to be more sensitive to erufosine.

Figure 6 presents the distribution of cells from the control cell line MCF-10A across various stages of the cell cycle. The control MCF-10A cells were exposed to the same concentrations of EPC3 as those used for the tumour MCF-7 cells. Erufosine does not cause significant alterations in the distribution of cells within the different phases of the cell cycle (Fig. 6).

The data obtained for the non-cancerous cell line indicate the presence of a "safety window," within which specific concentrations of erufosine are toxic to cancer cells while remaining relatively non-toxic to normal, non-cancerous cells.

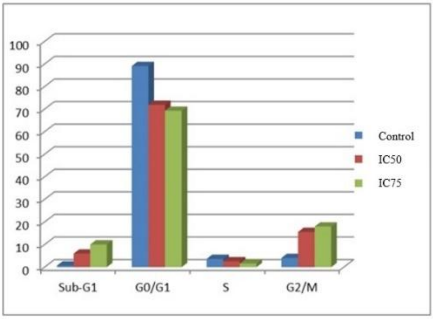

	Control	IC50	IC75
Sub-G1	0,71	10,05	58,7
G0/G1	89,1	69,3	28,7
S	3,65	1,6	1,2
G2/M	4,08	18	5,48

Fig. 6. *Flow cytometric analysis of the cell cycle of MCF-10A cells treated with erufosine for 48 h. The graph shows the distribution of cells across the cell cycle phases (Sub-G1, G0/G1, S, and G2/M).*

3. Dual AO/EtBr staining

Dual vital staining with a mixture of ethidium bromide and acridine orange was used to visualise viable, apoptotic, and necrotic cells after treatment with erufosine for 24 and 48 hours. Figure 7 shows untreated, viable cells from the cancer MDA-MB-231 cell line with normal morphology, fluorescing in the green spectral region. Treatment with IC_{25} of EPC3 for 24 h mainly induces early apoptotic changes in the cells. As treatment concentration increases, the cytotoxic effect of erufosine also increases. Treatment with IC_{50} for 48 hours results in a significant increase in the number of necrotic cells. In our earlier studies, we found that erufosine at IC_{50} concentration and higher doses also leads to apoptotic changes in the nuclei of Graffi cells isolated from a solid myeloid tumour in hamsters *[Georgieva A. et al., 2015]*. In addition to providing information on the dose range in which EPC3 induces apoptotic changes in MDA-MB-231 cancer cells, the present experiment also reveals a possible mechanism underlying this effect. In Fig. 7Z, a polyploid cell is observed, whose size is significantly larger due to erufosine-induced mitotic catastrophe resulting from G2/M phase cell cycle arrest. Similar results were reported by Kapoor V. and colleagues following treatment of oral squamous cell carcinoma cells *[Kapoor V., 2012]*.

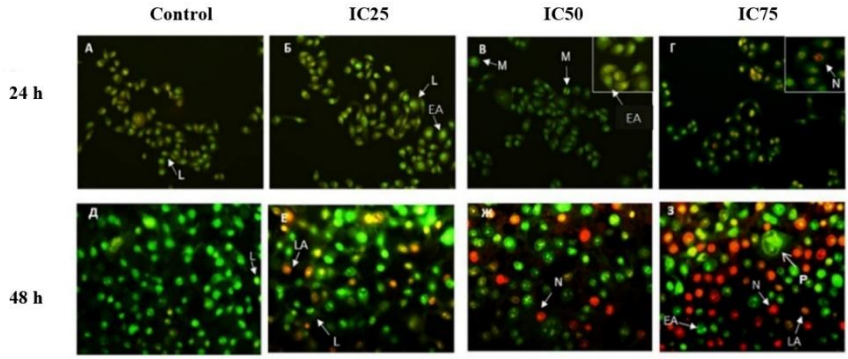

Fig. 7. AO/EtBr staining of MDA-MB-231 cells treated with different concentrations of erufosine for 24 and 48 hours. Viable cells (L), early apoptotic cells (EA), late apoptotic cells (LA), necrotic cells (N), cells in mitosis (M), and a polyploid cell (P). Microscopic magnification: 200× and 400×.

4. Flow cytometric analysis for the determination of apoptosis and necrosis in cells treated with erufosine

To quantitatively determine the type of cell death induced by erufosine, FACS analysis was performed on the tumour cell lines MDA-MB-231 and MCF-7, as well as on normal MCF-10A cells, treated with IC_{25}, IC_{50}, and IC_{75} for 24 and 48 hours.

In the highly invasive MDA-MB-231 cell line, a 5- and 9-fold increase in early apoptotic cells compared to the control was observed at 24 and 48 hours, respectively (Fig. 8). An increase in the number of late apoptotic cells was detected for the first time at 48 hours following treatment with the highest concentration, IC_{75}. No increase in necrotic cells was observed. These results confirm that erufosine induces apoptosis without triggering necrosis, which is a desirable property for potential antitumor agents.

Anexin V + / 7AAD - (Early apoptotic)				
EPC3	Control	IC25	IC50	IC 75
24ч.	0.71	1.62	2.2	3.5
48ч.	1.98	1.55	10.5	18.5
Anexin V + / 7AAD + (Late apoptotic / Necrotic)				
EPC3	Control	IC25	IC50	IC75
24ч.	1.51	0.91	0.92	1.52
48ч.	2.46	3.00	8.59	27.3
Anexin V - / 7AAD + (Necrotic)				
EPC3	контрола	IC25	IC50	IC 75
24ч.	0.8	0.7	1.15	1.35
48ч.	2.56	3.35	2.71	2.87

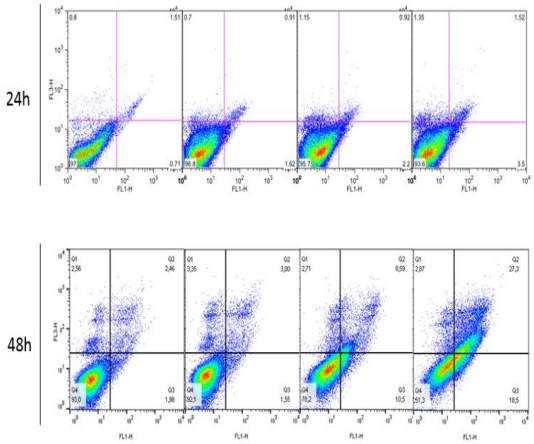

Fig. 8. Tabular and graphical presentation of the results from FACS analysis of MDA-MB-231 cells performed after 24- and 48-hour treatment with EPC3. The table shows the percentage distribution of cells undergoing early apoptosis, late apoptosis, or necrosis as a result of the treatment.

Anexin V + / 7AAD - (Early apoptotic)				
EPC3	контрола	IC25	IC50	IC 75
48ч.	0.58	6.98	7.02	6.24
Anexin V + / 7AAD + (Late apoptotic / Necrotic)				
EPC3	Control	IC25	IC50	IC75
48ч.	2.13	7.67	9.43	22.8
Anexin V - / 7AAD + (Necrotic)				
EPC3	Control	IC25	IC50	IC 75
48ч.	5.39	4.47	6.32	25.2

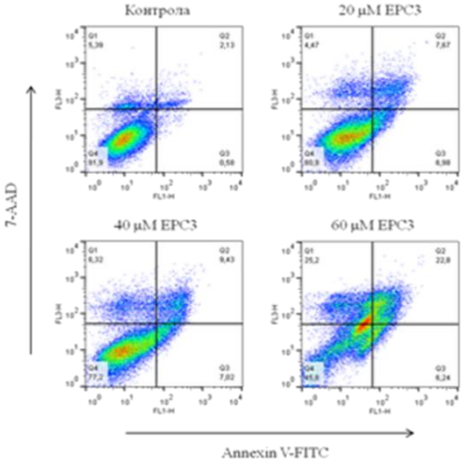

Fig. 9. Tabular and graphical presentation of the results from FACS analysis of MCF-7 cells performed after 48-hour treatment with EPC3. The table shows the percentage distribution of cells undergoing early apoptosis, late apoptosis, or necrosis as a result of the treatment.

Anexin V + / 7AAD - (Early apoptotic)				
EPC3	Control	IC25	IC50	IC75
48ч.	1.05	1.93	21.3	23.2
Anexin V + / 7AAD + (Late apoptotic / Necrotic)				
EPC3	контрола	IC25	IC50	IC75
48ч.	2.45	3.51	16.0	17.1
Anexin V - / 7AAD + (Necrotic)				
EPC3	контрола	IC25	IC50	IC75
48ч.	5.22	4.63	6.61	7.56

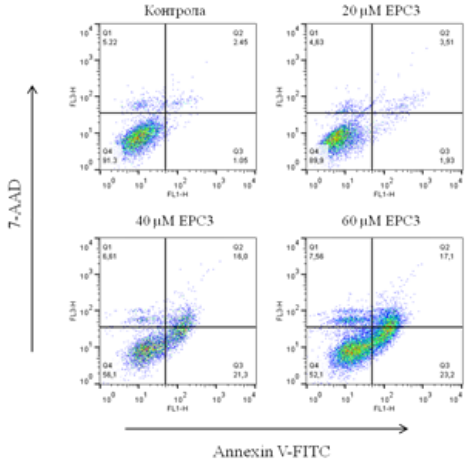

Fig. 10. Tabular and graphical presentation of the results from FACS analysis of MCF-10A cells performed after 48-hour treatment with EPC3. The table shows the percentage distribution of cells undergoing early apoptosis, late apoptosis, or necrosis as a result of the treatment.

In the MCF-7 cell line, 48-hour treatment with IC25 of EPC3 predominantly induces early apoptotic changes and, to a lesser extent,

late apoptotic changes (Fig. 9). Even after 48-hour treatment with IC75 of EPC3, the number of necrotic cells increases only about four times compared with the control. Similar to MDA-MB-231 cells, MCF-7 cells predominantly show an increase in early apoptotic cells following EPC3 treatment.

In the control MCF-10A cell line, 48 h of treatment with the highest EPC3 concentration predominantly increases the number of early apoptotic cells, while the number of necrotic cells remains unchanged (Fig. 10).

The performed FACS analysis confirms previous data indicating that EPC3 predominantly affects tumour cell lines, mainly inducing early apoptosis, with its effect being concentration- and time-dependent.

5. Effect of erufosine on the migratory potential of cancer cells

To investigate the effect of erufosine on the migratory potential of the MDA-MB-231 cell line, the wound-healing assay was used. The closure of the generated "wound" was monitored over 72 hours. The data are presented on Fig. 11 and 12.

After 5 hours of treatment, no significant changes were observed in the scratch area. At 24 hours, a decrease in migratory activity was observed in cells treated with IC50 and IC75 of EPC3 (Fig. 12). More than 50% inhibition of migratory potential was recorded at 48- and 72-hours following treatment with IC25 and IC50 of EPC3. The effect of EPC3 at 48 and 72 hours was dose-dependent.

The results suggest that erufosine is involved in regulating signalling pathways related to actin reorganisation, thereby affecting cell migration.

Its effect is likely connected to actin-binding proteins of the Rho family of small GTPases. Further support for this idea is provided by the results reported by Uzunova V. and colleagues, which indicate that treatment with erufosine suppresses RhoA expression.

The wound-healing assay demonstrated that, under in vitro conditions, erufosine reduces the migratory potential of MDA-MB-231 cancer cells.

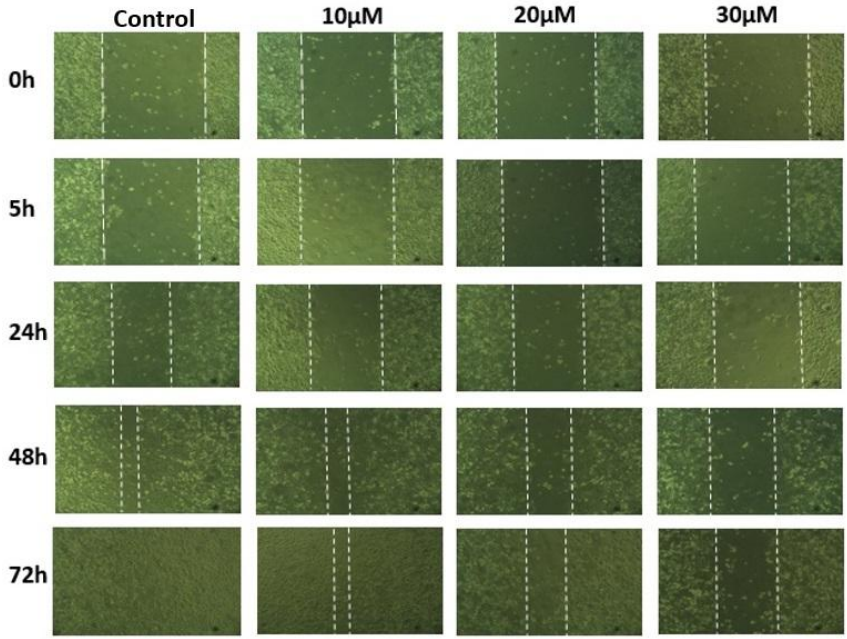

Fig. 11. Migration of MDA-MB-231 cells treated with different concentrations of erufosine. Images were acquired using a Leica DMI300B microscope (Leica Microsystems, Germany) at 100× magnification and processed in ImageJ. The images represent three independent experiments.

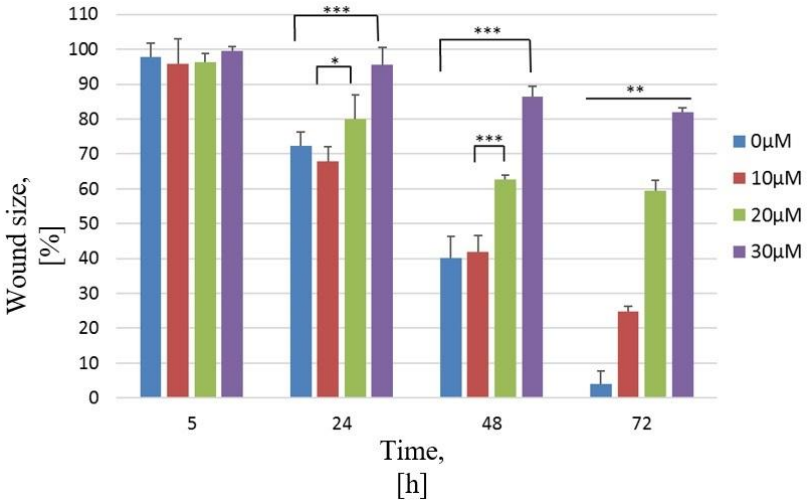

*Fig. 12. Reduction of the wound area measured over a period from 0 to 72 hours at different concentrations of erufosine. The data are normalised to the wound size at time 0. Statistical analysis was performed using one-way ANOVA followed by Tukey's post hoc test (*p < 0.05; **p < 0.01; ***p < 0.001).*

6. Effect of erufosine on the cytoskeletal organisation of MDA-MB-231 cells

To monitor changes in the actin cytoskeleton and cell nuclei in cells treated with erufosine, an experiment was performed in which cells were incubated for 24 hours with EPC3 at IC25, IC50, and IC75 concentrations (Fig. 13).

The highly invasive MDA-MB-231 cell line exhibits a mesenchymal mode of migration, characterised by strong cell adhesion and the presence of cytoskeletal protrusive structures. Such protrusive structures, including lamellipodia (Fig. 13A, thick arrow) and invadopodia (Fig. 13A, thin arrows), are observed in untreated cells.

Treatment with IC25 of EPC3 results in improved cell adhesion, as evidenced by clearly visible actin stress fibres (Fig. 13B, thin arrows). Additionally, the invadopodia depicted in Fig. 13B are associated with increased destructive activity towards the ECM.

Treatment of cells with IC50 of EPC3 causes disruption of actin filaments (Fig. 13C, arrows), and apoptotic changes appear in the nucleus (Fig. 13D, arrows). At the highest treatment dose – IC75 – actin filament disruption continues (Fig. 13D), and giant cells undergoing mitotic catastrophe are also observed (Fig. 13H, outlined nucleus).

The occurrence of mitotic catastrophe in cells treated with erufosine at IC50 and IC75 for 24 hours is the most likely cause of the significant increase in the proportion of apoptotic cells, as shown by FACS analysis (Fig. 8).

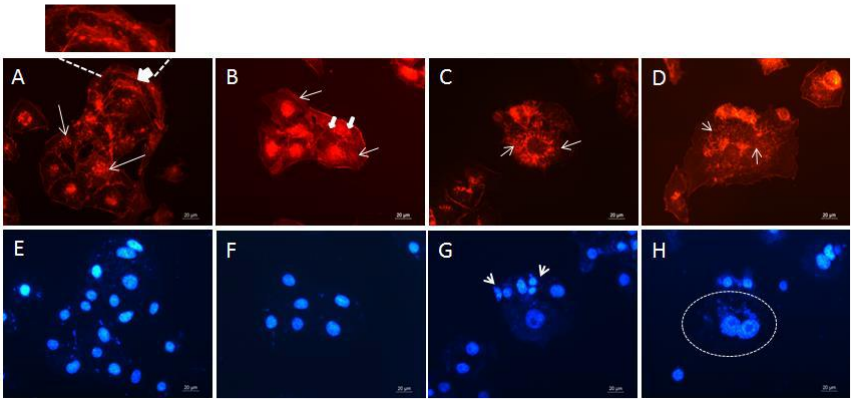

Fig. 13. Changes in actin cytoskeleton and nuclear organisation of MDA-MB-231 cells after treatment with erufosine. Cells were treated with EPC3 for 24 hours and stained for actin (red, upper panel) and DAPI for nuclei (blue, lower panel). A, E – untreated control cells; B, F – cells treated with IC25 EPC3; C, G – cells treated with IC50 EPC3; D, H – cells treated with IC75 EPC3.

7. Effect of Erufosine on the Fluidity of the Plasma Membrane in Cancer Cells

The effect of EPC3 on the fluidity and organisation of the plasma membranes of live tumour cells MDA-MB-231 and MCF-7 was examined using spectroscopic analysis with the fluorescent probe Di-4-ANEPPDHQ. The Di-4-ANEPPDHQ probe detects changes in membrane fluidity by shifting the emission maximum towards shorter wavelengths. This shift was quantitatively evaluated by calculating the General Polarisation (GP). Lower GP values indicate increased disorder and reduced lipid packing.

Treatment of cells with IC_{50} and IC_{75} doses of EPC3 for 24, 48, and 72 hours showed a time- and dose-dependent decrease in GP, indicating increased membrane fluidity. In MDA-MB-231 cells, GP decreased as early as 24 hours from approximately 0.55 in controls to around 0.25–0.30 in treated cells, and after 48 hours it reached approximately 0.15 at IC_{75} ($\Delta GP \approx -0.45$) (Fig. 14). A similar trend continued at 72 hours, with values steadily declining, confirming progressive disruption of lipid organisation.

In MCF-7 cells, the changes were less pronounced, with significant alterations observed only after prolonged treatment (72 hours) (Fig. 15). The widening of GP histograms with increasing treatment time indicates growing membrane heterogeneity, likely due to reorganisation of lipid domains and altered cholesterol distribution.

The experiment demonstrates that treatment with erufosine reduces the lipid order in the cell membrane in both cell lines, with a more pronounced effect in MDA-MB-231 cells.

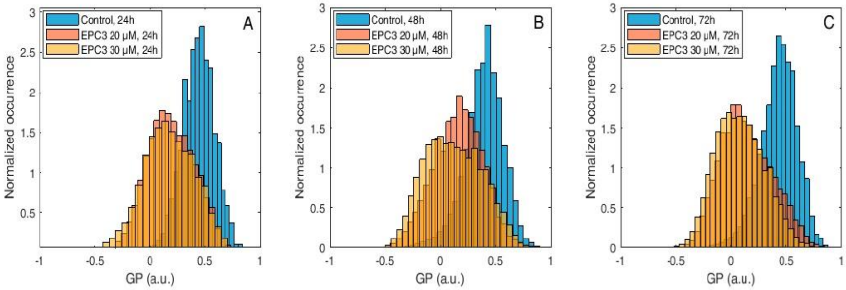

Fig. 14 GP Values (Di-4-ANEPPDHQ) Measured in the Plasma Membrane of MDA-MB-231 Cells Treated with EPC3. GP values were measured at the pixel level and are presented as normalized histograms. Cells were treated with IC_{50} (red) or IC_{75} (orange) of EPC3, as well as untreated cells (blue). Fluorescence intensity values were recorded after 24 hours (A), 48 hours (B), and 72 hours (C) of incubation with erufosine.

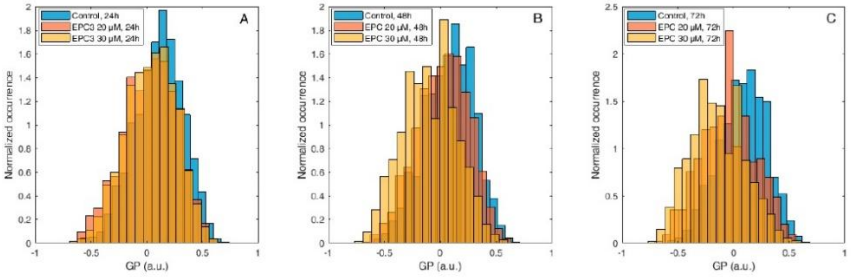

Fig. 15 GP Values (Di-4-ANEPPDHQ) Measured in the Plasma Membrane of MCF-7 Cells Treated with EPC3. GP values were measured at the pixel level and are presented as normalised histograms. Cells were treated with IC_{25} (red) or IC_{50} (orange) of EPC3, as well as untreated cells (blue). Fluorescence intensity values were recorded after 24 hours (A), 48 hours (B), and 72 hours (C) of incubation with erufosine. Two independent experiments were performed.

8. Effect of Erufosine on Phospholipid and Cholesterol Content in Cell Membranes

The effect of erufosine on the concentrations of various phospholipids and cholesterol in cell membranes of MDA-MB-231 and MCF-7 cells was examined using thin-layer chromatography and gas chromatography. Cells were treated with IC_{50} and IC_{75} of EPC3 for 24 hours.

The experiment demonstrated that, in both cell lines, increasing erufosine concentration significantly decreased sphingomyelin (SM) content (Fig. 16A and 16 B). Moreover, the results show that erufosine reduces phosphatidylcholine (PC) levels in both cancer cell lines (Fig. 16C and D). In MCF-7 cells treated with IC_{75} of EPC3, PC decreased by 20% relative to control, whereas in MDA-MB-231 cells, the decrease was 17%. The inhibition of PC synthesis is one pathway that induces apoptosis. Conversely, the level of phosphatidylserine (PS) increased in both cancer cell lines treated with erufosine (Fig. 16A and B). Elevated PS levels in the outer leaflet of the cell membrane are linked to the initiation of apoptosis and have been observed in cancer cells following chemotherapy or radiotherapy [*Birge R.B. et al., 2016].*

As shown in Fig. 16A and B, treatment with IC_{75} of erufosine also lowered cholesterol levels in the membranes of MDA-MB-231 and MCF-7 cells, which is associated with reduced cell migration and survival.

Based on these results, it can be suggested that the cytotoxic effect of erufosine is related to its impact on membrane organisation,

specifically by reducing the stability and quantity of ordered lipid domains.

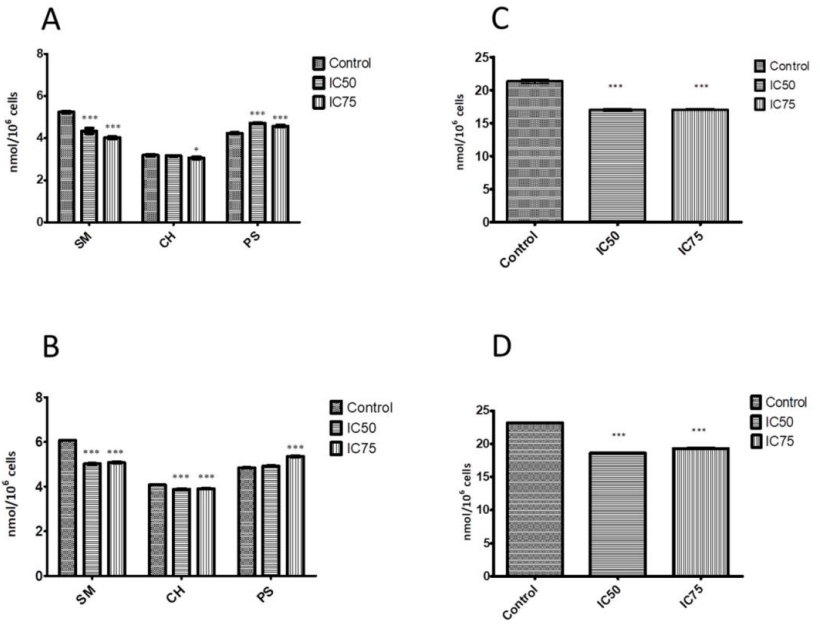

*Fig. 16. Effect of EPC3 on SM, CH, PS, and PC Levels in Cell Membranes. (A) Levels of SM, CH, and PS in MCF-7 cells treated with EPC3 for 24 hours; (B) Levels of SM, CH, and PS in MDA-MB-231 cells treated with EPC3 for 24 hours; (C) Levels of PC in MCF-7 cells treated with EPC3 for 24 hours; (D) Levels of PC in MDA-MB-231 cells treated with EPC3 for 24 hours. The graphs show the mean values from three independent experiments. Statistical significance was calculated relative to the controls for each group using one-way ANOVA followed by Bonferroni's test. *p < 0.01 and ***p < 0.0001.*

9. Effect of Erufosine on the Diffusion Dynamics of Transmembrane Proteins in the Plasma Membrane

The effect of erufosine on the diffusion dynamics of two proteins—the human epidermal growth factor receptor (hEGFR) and influenza A

virus haemagglutinin (FPV-HA)—was examined in MDA-MB-231 cells treated with IC_{75} of EPC3. EGFR is localised to lipid domains of the plasma membrane [Bag N. et al., 2015] and is crucial for cancer development and progression [Sigismund S. et al., 2018]. The second protein, FPV-HA, resides in raft domains and influences the diffusion dynamics of the plasma membrane [*Takeda M. et al., 2003; Scheiffele P. et al., 1999; McKay T. et al., 2006*].

Fluorescence microscopy studies showed that erufosine does not alter the localisation of these proteins in the membrane but significantly increases their diffusion dynamics (Fig. 17). To quantitatively assess the diffusion of both proteins, scanning fluorescence correlation spectroscopy was applied. The calculated diffusion coefficients increased approximately fivefold for both hEGFR (from 0.26 ± 0.08 to 1.1 ± 0.5 $\mu m^2/s$-1) and FPV-HA (from 0.22 ± 0.08 to 1.2 ± 0.5 $\mu m^2/s$-1), indicating enhanced membrane fluidity and reduced stability of lipid domains (Fig. 17C).

These results confirm that erufosine modifies the physical properties of the plasma membrane by altering lipid–lipid and lipid–protein interactions, initially disrupting lipid bilayer organisation and subsequently affecting membrane lipid metabolism and composition.

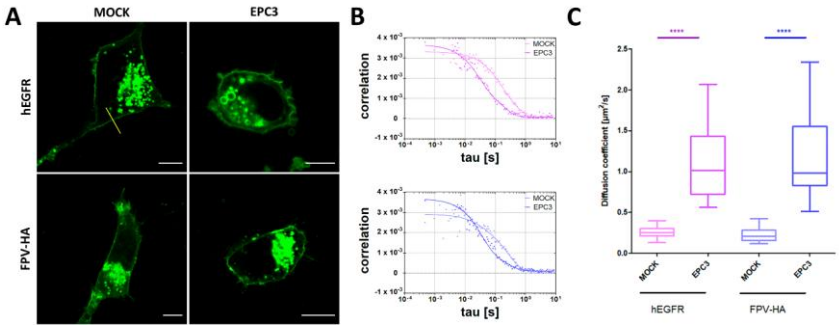

*Fig. 17. Quantitative Assessment of Protein Diffusion in MDA-MB-231 Cells Treated with Erufosine. (A) Confocal fluorescence microscopy images of MDA-MB-231 cells expressing hEGFR-EGFP (top row) and FPV-HA-EGFP (bottom row), in the absence of erufosine and after 48 hours of treatment with erufosine. The yellow line in (A) indicates the scan path used for sFCS measurements. Scale bar: 10 µm. (B) sFCS autocorrelation functions and fits obtained from cells expressing hEGFR-EGFP (top graph) and FPV-HA-mEGFP (bottom graph), in the absence of erufosine and after 48 hours of treatment with erufosine. (C) Box plot of diffusion coefficients calculated based on sFCS diffusion times, obtained from three independent experiments (each including measurements of 20 cells). All measurements were performed at room temperature. ****p < 0.0001.*

Part II. Investigation of the Effect of Miltefosine and DMS on A549 and HUVEC Cell Lines

In the second part, we present the results of experiments conducted on A549 and HUVEC cell lines. The effects of DMS and HePC on cell viability, cytoskeleton organisation, type of induced cell death, cell morphology, intracellular S1P levels, and the degree of genotoxicity were investigated. The action of both agents was studied under single and combined treatments.

1. Effect of Miltefosine and/or DMS on the Viability of A549 Cells

An MTT assay was performed to evaluate the effect of miltefosine (HePC) and dimethylsphingosine (DMS) on the viability of A549 lung carcinoma cells and non-cancerous HUVEC cells. Based on the results, IC_{50} values were calculated at 24 and 48 hours and subsequently used for combination treatments.

The results indicate that DMS exhibits greater cytotoxicity than miltefosine in both cancer cell lines, and its effect is dependent on time and dose (Fig. 18A). After 24 hours of treatment with 40 µM DMS, about 50% inhibition of cell growth was observed, while after 48 hours, the same effect was achieved with 20 µM (Fig. 18A).

Miltefosine exerted its inhibitory effect at notably higher concentrations compared to DMS. The calculated IC_{50} values for DMS ranged from 212 to 277 µM at 24 h and from 192 to 268 µM at 48 h (Fig. 18D).

In HUVEC cells, the calculated IC_{50} values for DMS were higher than those in A549 cells, indicating that normal cells are less sensitive to DMS's cytotoxicity. In contrast, HUVEC cells were more sensitive to HePC than A549 cells (Fig. 19D), which is unsurprising given the well-documented strong side effects of this antitumour agent [*Jiménez-López J.M. et al., 2010*].

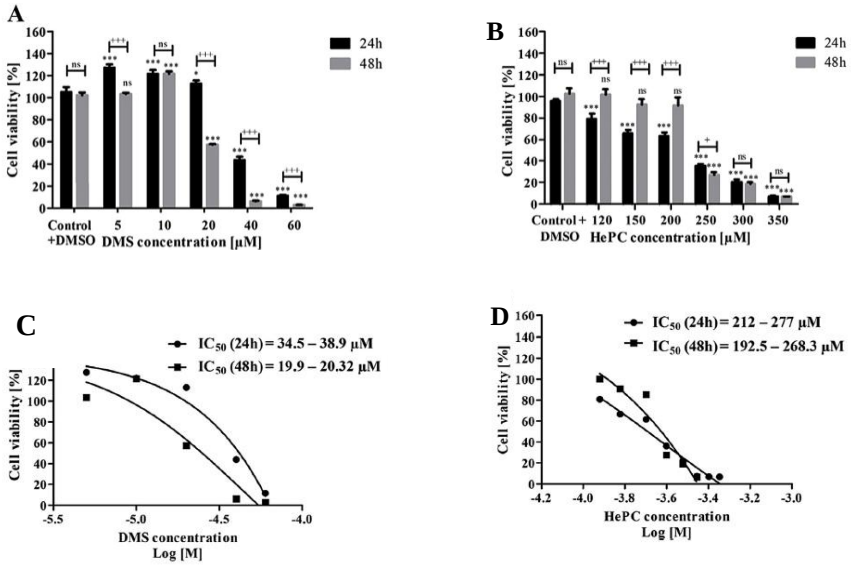

*Fig. 18. Viability of A549 Cancer Cells Treated for 24 and 48 h with DMS at Concentrations of 5–60 µM (A) and HePC at Concentrations of 120–350 µM (B). DMS IC_{50} (C) and HePC IC_{50} (D) were calculated for 24 and 48 h using GraphPad Prism. Statistical significance is shown as comparisons between treated cells and control cells (***) and between 24 h and 48 h treatments (+++), with ***$p < 0.001$, *$p < 0.05$, and +++$p < 0.001$.*

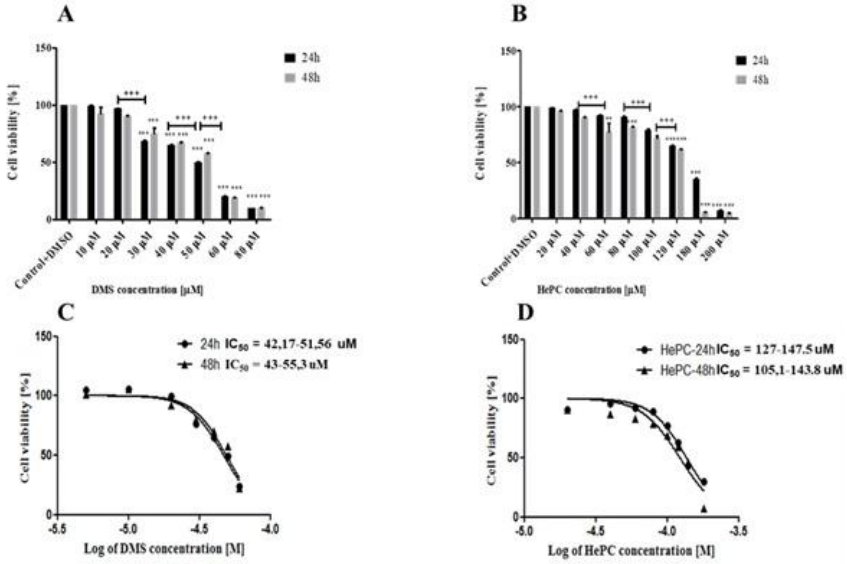

*Fig. 19. Viability of HUVEC Cells Treated for 24 and 48 h with DMS at Concentrations of 10–80 µM (A) and HePC at Concentrations of 20–200 µM (B). DMS IC_{50} (C) and HePC IC_{50} (D) were calculated for 24 and 48 h using GraphPad Prism. Statistical significance is shown as comparisons between treated cells and control cells (*) and (), and between 24 h and 48 h treatments (+++), with ***p < 0.001, **p < 0.01, and +++p < 0.001.*

2. Treatment of A549 and HUVEC Cells with a Combination of Miltefosine and DMS

For the first time within the framework of this dissertation, a combined treatment with miltefosine and dimethylsphingosine was conducted to investigate a potential synergistic cytotoxic effect and to reduce the side effects characteristic of single miltefosine administration *[Jiménez-López J.M. et al., 2010]*.

A549 lung cancer cells were treated with three different combinations of miltefosine and DMS: HePC IC50 + DMS IC25, HePC IC25 + DMS IC50, and HePC IC25 + DMS IC25 (Fig. 20A). The most effective effect on reducing cell viability was shown by the combinations HePC IC25 + DMS IC25 and HePC IC25 + DMS IC50, and after longer treatment (48 h), their cytotoxic effect continued to increase (Fig. 20A). The results show that the combined treatment with HePC and DMS leads to a significant decrease in cell viability of A549 lung carcinoma cells, with the effect being synergistic and stronger compared to individual treatments. In the control HUVEC cell line, the combination treatment exhibited a weaker suppressive effect, suggesting selectivity of action towards tumour cells. These results support the potential of the combination approach as a more effective and less toxic strategy for inhibiting tumour growth.

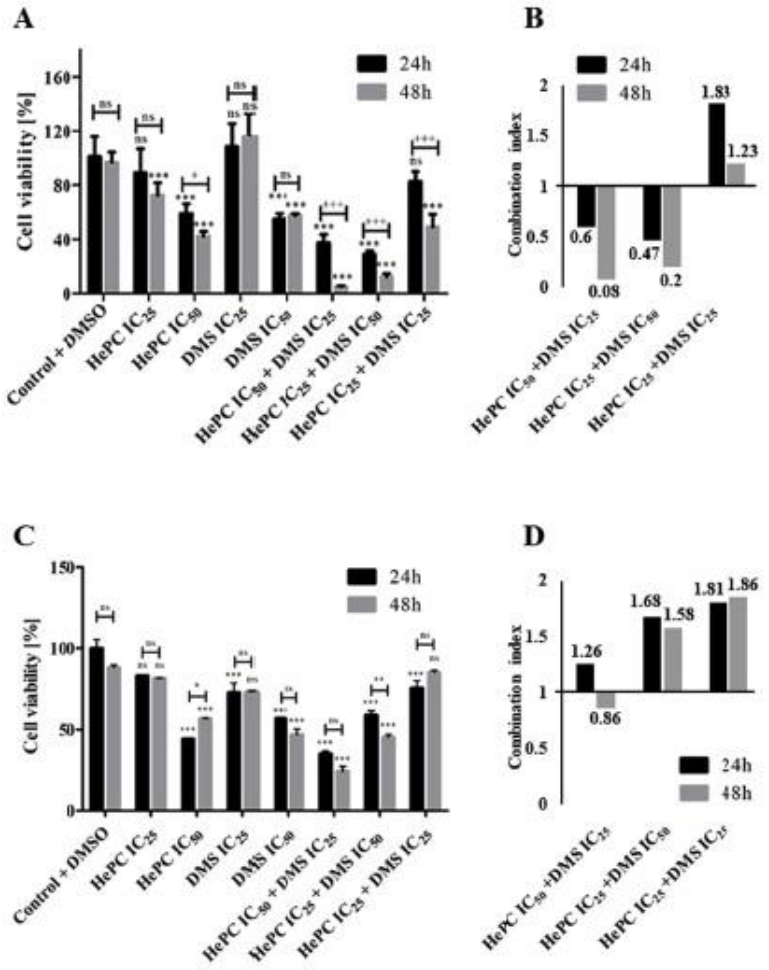

*Fig. 20. Viability of A549 Cancer Cells (A) and HUVEC Cells (C) Treated with Different Combinations of HePC and DMS for 24 and 48 h. The combination index (CI) was calculated for the combined treatments of DMS and HePC at 24 and 48 h in A549 (B) and HUVEC (D). The graphs show mean values obtained from three independent experiments. Statistical significance is presented as comparisons between treated cells and control (***) and as comparisons between 24 h and 48 h treatments (+++), with ***p < 0.001, *p < 0.05, +++p < 0.001, ++p < 0.01, +p < 0.05.*

3. Synergistic Inhibitory Effect of Miltefosine and DMS on Cell Viability, Expressed by the Combination Index

To assess the interaction between miltefosine and DMS, the combination index (CI) was determined for 24- and 48-hour combined treatments of A549 and HUVEC cells. The analysis indicated that in A549 cells, combining HePC IC_{50} with DMS IC_{25} (CI = 0.6) and HePC IC_{25} with DMS IC_{50} (CI = 0.47) showed significant synergism (CI < 1), which grew more pronounced with longer treatment times. The most notable synergistic effect was observed after 48 hours for the combination HePC IC_{50} + DMS IC_{25}.

In the control HUVEC cell line, treatment with miltefosine and DMS did not show a synergistic effect, except for the combination HePC IC_{50} + DMS IC_{25}, which exhibited a modest synergistic effect only after 48 hours of treatment (CI = 0.86) (Fig. 20D).

These data confirm the results of the MTT assays and indicate that the combined application of miltefosine and DMS exerts a time-dependent synergistic cytotoxic effect on A549 tumour cells.

4. Combined Effect of Miltefosine and DMS on the Morphology of A549 and HUVEC Cells

To evaluate morphological changes induced by combined miltefosine and DMS treatment, phase-contrast microscopy was performed on A549 and HUVEC cells.

Single-agent treatments with either compound resulted in cell rounding and a decrease in cell number, while the combined treatments caused a more significant reduction in cell density and a notable increase in

apoptotic cells (Fig. 21). The experiment confirmed previous findings, showing that the inhibitory effect of combined HePC and DMS treatments on A549 cells depends on time (Fig. 21B). This is also evident in Fig. 21C, which displays cell counts after 24 and 48 hours of treatment with each combination.

5. DAPI Staining of A549 Cell Nuclei Following Treatment with HePC and DMS

The pro-apoptotic effects of miltefosine and DMS were assessed by DAPI staining and fluorescence microscopy of A549 cells. Control cells did not exhibit nuclear changes after 24 or 48 h. Single-agent treatment with DMS IC_{50} or HePC IC_{50} induced characteristic apoptotic changes, including nuclear blebbing after 24 h (Fig. 22A) and the formation of apoptotic bodies after 48 h (Fig. 22B). Combined treatments triggered apoptosis as early as 24 h, with the strongest effect observed for the HePC IC_{50} + DMS IC_{25} combination (Fig. 22A). These results confirm the previously observed synergistic cytotoxic potential of the two agents.

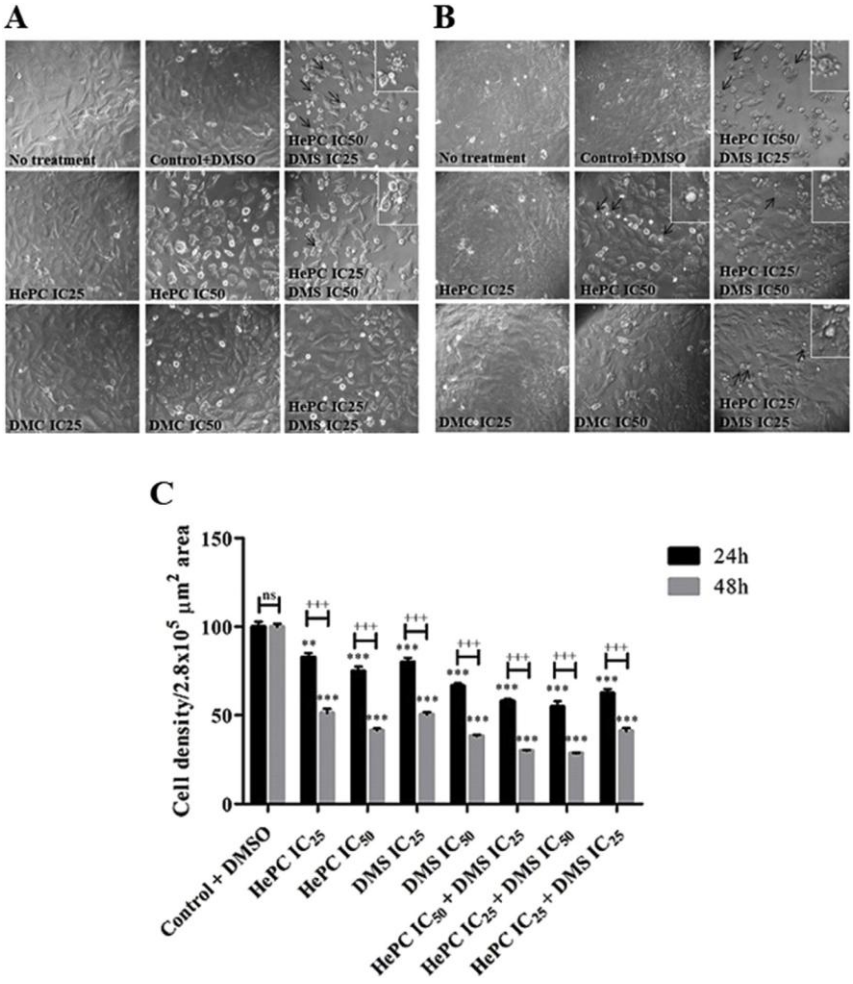

*Fig. 21. Phase-contrast microscopy of A549 lung carcinoma cells treated with HePC and DMS in different combinations. Cells were incubated for 24 (A) and 48 (B) hours. Magnification: 20×. Cell counts per field after 24 and 48 h for each individual treatment are shown in (C). The figure presents mean values from three independent experiments. Statistical significance is indicated by comparisons between treated cells and controls (***) and between 24 h and 48 h treatments (+++). ***p < 0.001; **p < 0.01; +++p < 0.001.*

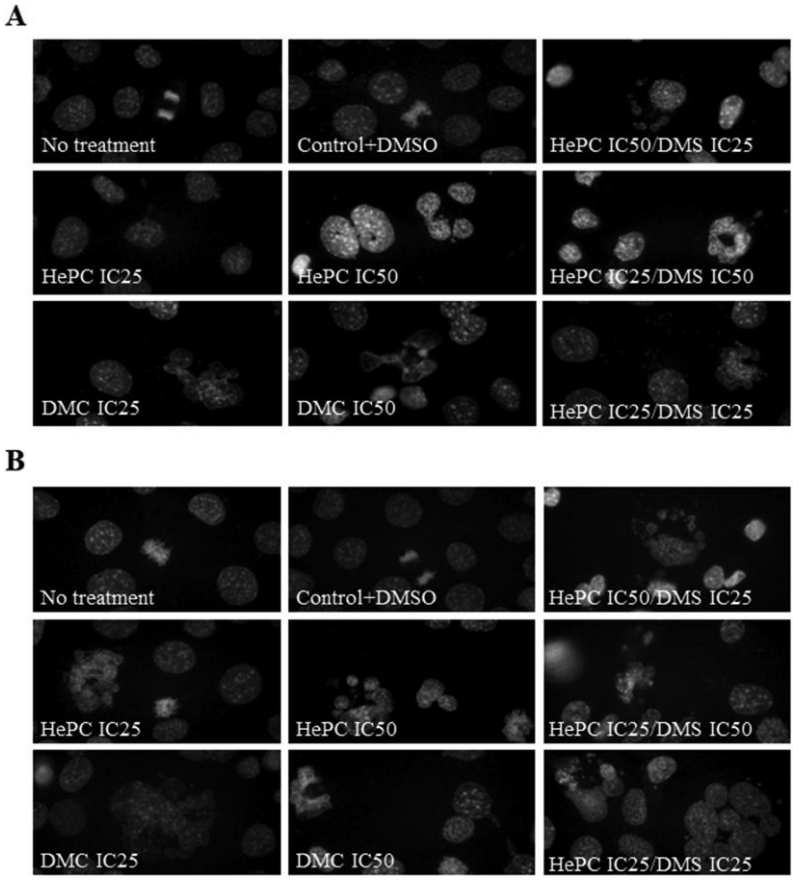

Фиг.22 Оцветяване с DAPI на ракови клетки A549 от бял дроб, след 24 ч. (А) и 48 ч. (Б) третиране с DMS и HePC. Увеличение на обектива 100х.

6. FACS Analysis of Apoptosis/Necrosis Induction in A549 and HUVEC Cells Treated with HePC and DMS

To identify the type of cell death induced by miltefosine and DMS, flow cytometry was performed on A549 and HUVEC cells after 24 hours of treatment.

In A549 cells, the strongest early apoptotic effect was observed after treatment with DMS IC_{50} (8.25%), whereas late apoptosis/necrosis was most pronounced following the combination of HePC IC_{50} + DMS IC_{25} (66%) where the effect is synergistic (Fig. 23A). Notably, the number of necrotic cells resulting from the HePC IC_{50} + DMS IC_{25} combination was significantly lower compared to necrosis observed after single-agent HePC IC_{50} treatment. These findings are consistent with the synergy previously observed in the MTT analysis.

In HUVEC cells, treatment with HePC and DMS primarily increased early and late apoptosis, without a significant increase in necrosis. The strongest apoptotic effect was observed with the HePC IC_{25} + DMS IC_{50} combination, followed by DMS IC_{50} alone. These results confirm that the combined application of the two agents is more cytotoxic to A549 tumour cells than to normal HUVEC cells.

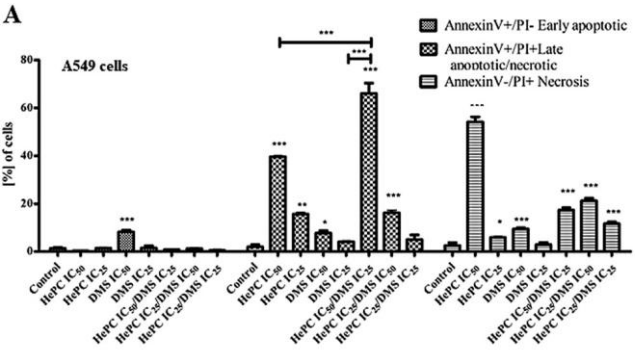

	Early apoptotic	Annexin V+/PI+ Late apoptotic/necrotic	Annexin V-/PI+ Necrotic
Control	1.36±0.67	2.02±1.28	2.54±1.58
HePC IC50	0.34±0.007	39.65±0.28	54.17±2.92
HePC IC25	1.41±0.16	15.65±0.67	6.00±0.14
DMS IC50	8.25±1.12	7.75±1.46	9.48±0.66
DMS IC25	1.56±1.24	4.10±0.25	2.90±1.29
HePC IC50/ DMS IC25	0.83±0.07	66.10±6.02	17.33±1.51
HePC IC25/ DMS IC50	1.26±0.13	16.24±1.94	21.23±1.53
HePC IC25/ DMS IC25	0.53±0.21	5.05±2.72	11.65±1.06

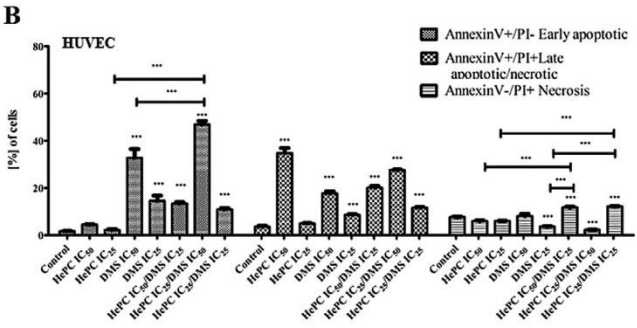

	Annexin V+/PI-	Annexin V+/PI+ Late apoptotic/necrotic	Annexin V-/PI+ Necrotic
Control	1.67±0.24	3.55±0.63	7.68±0.36
HePC IC50	4.49±0.21	34.78±2.92	5.95±0.40
HePC IC25	2.22±0.43	4.97±0.30	6.01±0.13
DMS IC50	32.75±5.25	17.64±1.30	8.15±1.23
DMS IC25	14.57±3.01	8.59±0.45	3.62±0.27
HePC IC50/ DMS IC25	13.39±0.72	20.07±1.01	11.74±0.49
HePC IC25/ DMS IC50	46.86±2.13	27.54±0.27	2.33±0.02
HePC IC25/ DMS IC25	10.89±0.71	11.61±0.37	12.20±0.16

Fig. 23. Representative FACS data for the detection of apoptosis/necrosis in A549 (A) and HUVEC (B) cells. Cells were incubated with HePC and DMS.

7. CBMN Analysis

A CBMN assay was conducted on A549 cancer cells to evaluate the genotoxic effects of HePC and DMS, both individually and in combination (HePC IC_{25} + DMS IC_{25}). The results did not show a significant genotoxic impact, based on the frequency of binucleated cells and the presence of micronuclei, nucleoplasmic bridges, and nuclear buds in 500 binucleated cells (Table 3).

*Table 3. Effect of DMS IC_{25}, HePC IC_{25}, HePC IC_{25} + DMS IC_{25}, and Mitomycin C on the frequency of micronuclei (MN), nucleoplasmic bridges (NPB), and nuclear buds (NB) in 500 binucleated cells (BNCs) of A549. All CBMN biomarkers were evaluated at 1000× magnification using a Jena Lumar optical microscope (Germany). Results were obtained from three independent experiments (**P < 0.01 and ***P < 0.001).*

Biomarker	Control	DMS IC_{25}	HePC IC_{25}	HePC IC_{25} + DMS IC_{25}	Mitomycin C
MN	11.38±1.11	12.06±1.71	13.59±1.63	12.45±0.97	35.80±0.83***
NPB	12.74±2.23	13.41±1.22	15.31±2.14	13.93±2.58	21.97±2.79**
NB	0.99±0.27	1.31±0.21	1.63±0.41	1.47±0.62	1.75±0.41

8. Results of Sphingosine-1-Phosphate (S1P) Analysis

Due to the key role of S1P in the sphingolipid rheostat *[Strub G.M. et al., 2010]* and in tumour progression, we investigated changes in its levels induced by HePC and DMS, applied individually or in combination.

In A549 cells treated separately with DMS or miltefosine, a significant reduction in S1P levels was observed (Fig. 24 A). Combined treatment exhibited a synergistic effect on S1P reduction, which was most pronounced following exposure to the combination HePC IC_{50} + DMS IC_{25}, followed by HePC IC_{25} + DMS IC_{50} (Fig. 24 A). These findings are consistent with the results from the MTT assay, microscopy observations, and FACS analysis, collectively demonstrating a synergistic effect of the combined agents on inducing cytotoxicity and apoptosis.

To clarify the relationship among miltefosine, PKC, and SK1, cells were treated with miltefosine, followed by PKC activation with phorbol 12-myristate 13-acetate (PMA). It was found that PMA partially restored S1P production suppressed by miltefosine. Immunoblot analysis confirmed this mechanism, showing a significant decrease in phosphorylated PKCα after miltefosine treatment (Fig. 25A and 25 B).

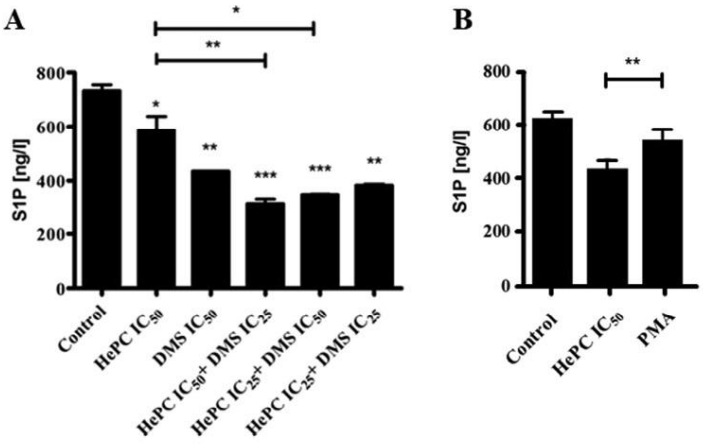

*Fig. 24. ELISA measurement of S1P levels in A549 cells. (A) Control cells were incubated with DMSO only, while the remaining cells were treated with miltefosine and/or DMS for 24 h. (B) Control cells, cells treated with miltefosine, and cells treated with PMA. Results represent the mean of three independent experiments, each performed in quadruplicate (*p < 0.05; **p < 0.01; ***p < 0.001).*

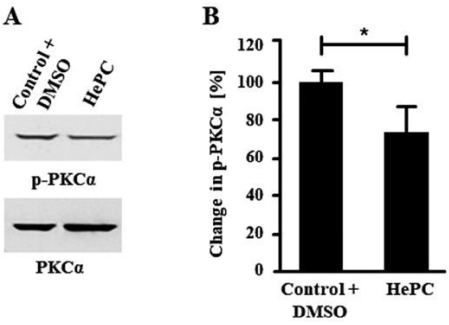

*Fig. 25. Changes in PKCα phosphorylation induced by HePC. (A) Immunoblot analysis of phosphorylated PKCα in A549 cells treated with Control + DMSO or HePC IC50 for 24 hours. (B) Graphical representation of changes in PKCα phosphorylation (expressed as percentages). Results are shown as the mean of three independent experiments. *p < 0.05.*

9. Assay for Cytochrome C Reductase (NADPH) Activity

To evaluate the pro-apoptotic potential of miltefosine and DMS, cytochrome c reductase activity was assessed in A549 cells. Cytochrome C reductase participates in the mitochondrial electron transport chain. Changes in its activity can lead to the formation of pores in the outer mitochondrial membrane, release of cytochrome C into the cytosol, and activation of apoptosis.

The highest level of absorbance was observed with treatment using HePC IC50 + DMS IC25, followed by the other two combination treatments (Fig. 26A). The calculated enzymatic activity confirmed these findings: single treatments with HePC IC50 or DMS IC50 resulted in significantly lower cytochrome C reductase activity compared to the combined treatments (Fig. 26B). The most notable synergistic effect was seen with the HePC IC50 + DMS IC25 combination (Fig. 26B). These data suggest that the combination of HePC IC50 + DMS IC25, followed by HePC IC25 + DMS IC50, has the greatest potential to induce apoptosis through the mitochondrial apoptotic pathway.

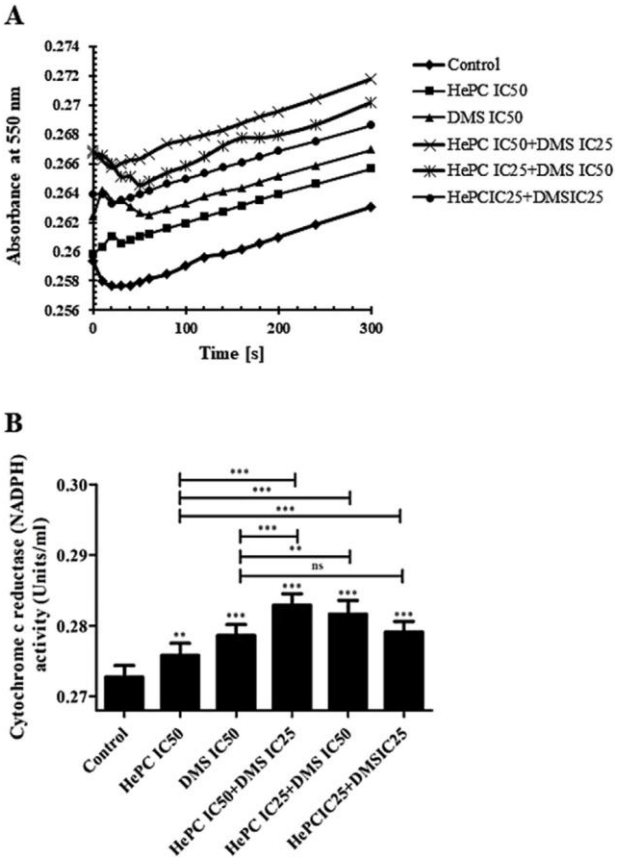

*Fig. 26. Cytochrome C Reductase (NADPH) Activity in A549 Cells Activity was measured in A549 cells treated with HePC and DMS, either alone or in combination, for 24 h. Absorbance at 550 nm for the different treatments (A), and cytochrome C reductase activity (B). Results represent the mean values from three independent experiments. ***p < 0.001, **p < 0.01.*

Chapter 5. Conclusion

Based on the results obtained, we established that the alkylphosphocholines erufosine and miltefosine can be effectively used for treating aggressive breast and lung tumours. We demonstrated that erufosine inhibits the proliferation and migration of breast cancer cells and, for the first time, revealed a connection between these effects and alterations in the physicochemical properties of cellular membranes. Furthermore, the findings clearly indicate that this alkylphosphocholine preferentially targets the highly invasive MDA-MB-231 cell line, making it a promising antitumour agent for treating highly aggressive breast tumours.

In this dissertation, we demonstrated for the first time that miltefosine can be successfully used to treat lung cancer as part of a combined therapy with dimethylsphingosine. Both antitumor lipids exhibit a synergistic inhibitory effect on the viability and proliferation of A549 cancer cells, predominantly inducing apoptosis. The combined treatment resulted in a significantly stronger inhibitory effect at lower miltefosine doses, addressing one of the main problems of conventional anticancer therapies—high toxicity to non-cancerous cells and severe side effects.

These results uncover new therapeutic options for treating breast and lung cancer—types of cancer with the highest social impact.

Chapter 6. Main Conclusions

In the present dissertation, the mechanism of action of antitumor lipids on transmembrane signalling in breast and lung cancer cells, as well as the induction of apoptosis, was investigated. The objectives were addressed in two parts of the dissertation: the first covering six tasks and the second, three.

In **Part I**, the effect of erufosine on the tumour cell lines MDA-MB-231, MCF-7, and the normal cell line MCF-10A was examined. Based on the obtained results, it can be concluded that erufosine is a suitable antitumor agent, which:

- exhibits cell-specific cytotoxic activity in breast cancer cells, with a more pronounced effect in the highly invasive cell line.
- induces apoptosis in a concentration-dependent manner
- causes cell cycle arrest at the G2/M phase
- induces destruction of protrusive cytoskeletal structures and reduces cell migratory potential
- reduces the order of the cell membrane's lipid bilayer and improves protein diffusion across it (more notable in MDA-MB-231)

In Part II, the effect of miltefosine and DMS on the A549 and HUVEC cell lines was examined. Based on the results, conclusions were drawn regarding their mechanisms of action and the potential for developing

combined therapies for lung cancer treatment. The experiments clearly show that the combination of miltefosine and DMS causes:

- a pronounced synergistic cytotoxic effect on lung cancer cells
- late apoptosis in cancer cells via activation of the intrinsic apoptotic pathway
- a decrease in S1P levels in lung cancer cells

Chapter 7. Contributions

I. Original Contributions

Contributions related to **Part I** of the dissertation:

1. 1. For the first time, a direct link has been demonstrated between changes in lipid composition, lipid layer ordering, and the diffusion dynamics of the cell membrane under the action of erufosine, as well as alterations in the cell cycle at the G2/M phase and the induction of apoptosis in the highly metastatic breast cancer cell line MDA-MB-231.

Contributions related to **Part II** of the dissertation:

1. For the first time, it has been established that combined treatment with HePC and DMS demonstrates a synergistic cytotoxic effect on lung cancer cells.
2. Combined treatment with HePC and DMS inhibits signalling pathways linked to sphingosine kinase 1 (SK1) and protein kinase C (PKC), lowers S1P levels in cancer cells, and triggers apoptosis via the intrinsic mitochondrial pathway.

II. Applied Contributions

1. The high selectivity of the alkylphosphocholines used (erufosine and miltefosine) toward the highly metastatic breast cancer cell line MDA-MB-231 and the lung cancer cell line A549, along with their

minimal effect on normal MCF-10A and HUVEC cells, provides a basis for their potential application in modern anticancer therapy.

2. The discovered synergistic cytotoxic effect of the miltefosine and DMS combination on tumour cells enables higher therapeutic efficacy at lower miltefosine doses, reducing side effects.

Chapter 8. List of Publications Related to the Dissertation

1. **Stoyanova, T**., Uzunova, V., Momchilova, A., Tzoneva, R., Ugrinova I. (2021). The treatment of breast cancer cells with erufosine leads to actin cytoskeleton reorganization, inhibition of cell motility, cell cycle arrest and apoptosis. Comptes rendus de l'Académie bulgare des Sciences, 74(1), 88–94, Q3
2. Tzoneva, R.; **Stoyanova, T.;** Petrich, A.; Popova, D.; Momchilova, A.; Chiantia, S. (2020). Effect of Erufosine on Membrane Lipid Order in Breast Cancer Cell Models. Biomolecules, 10(5), 802, Q2
3. Uzunova, V.; Tzoneva, R.; **Stoyanova, T**.; Pankov, R.; Skrobanska, R.; Georgiev, G.; Maslenkova, L.; Tsonchev, Z.; Momchilova, A. (2019). Dimethylsphingosine and Miltefosine Induce Apoptosis in Lung Adenocarcinoma A549 Cells in a Synergistic Manner. Chem.-Biol. Interact., 310, 108731, Q1

Chapter 9. Citations of the author's publication

Tzoneva, R.; Stoyanova, T.; Petrich, A.; Popova, D.; Momchilova, A.; Chiantia, S. (2020). Effect of Erufosine on Membrane Lipid Order in Breast Cancer Cell Models. Biomolecules, 10(5), 802.

Citing Articles

1. Pfeil-Gardiner, O., Rosa, H. V. D., Riedel, D., Chen, Y. S., et al. (2024). Elemental mapping in single-particle reconstructions by reconstructed electron energy-loss analysis. Nature, 630(8019), 123–129
2. Xu, Z., Chu, M. (2022). Advances in immunosuppressive agents based on signal pathway. Frontiers in Pharmacology, 13, 890123.
3. Mollinedo, F., Gajate, C. (2021). Mitochondrial targeting involving cholesterol-rich lipid rafts in the mechanism of action of the antitumor ether lipid and alkylphospholipid analog edelfosine. Pharmaceutics, 13(5), 763.
4. Silva, P. M., da Silva, I. V., Sarmento, M. J., Silva, Í. C., Carvalho, F. A., Soveral, G., Santos, N. C. (2022). Aquaporin-3 and aquaporin-5 facilitate migration and cell–cell adhesion in pancreatic cancer by modulating cell biomechanical properties. *Cells*, 11(8), 1308.
5. Küçüksayan, E., Sansone, A., Chatgilialoglu, C., Ozben, T., Tekeli, D., Talibova, G., Ferreri, C. (2022). Sapienic Acid Metabolism Influences Membrane Plasticity and Protein Signaling in Breast Cancer Cell Lines. *Cells*, 11(2), 225.
6. Sarangi, N. K., Prabhakaran, A., Keyes, T. E. (2020). Interaction of Miltefosine with Microcavity Supported Lipid Membrane: Biophysical insights from electrochemical impedance spectroscopy. *Electroanalysis*, 32(12), 2936–2945
7. liev, I., Mavrova, A., Yancheva, D., Dimov, S., Staneva, G., Nesheva, A., Tsoneva, I., Nikolova, B. (2023). 2-Alkyl-Substituted-4-Amino-Thieno[2,3-d]Pyrimidines: Anti-Proliferative Properties to In Vitro Breast Cancer Models. *Molecules*, 28(17), 6347.
8. Shafiq, N., Iqbal, U. U., Javed, A., Pervaiz, A. (2025). Alkyl-phospholipid mediated toxicity and regulation of transcriptomic profile of cell cycle genes in liver cancer cells. *Biomedical Current Research, 2(1).*

9. T Mandal (2024). Unraveling the Molecular Mechanisms of Hepatitis C Virus Assembly, Universität Potsdam, Potsdam, December 11 , PhD thesis.
10. Akhtar, M. S., Ali, S. S. (2024). Erufosine alters the genes associated with G2/M Phase of cell cycle in cancers: Molecular evidence from gene expression analysis. *Biomedical Current Insights*, 1(2).
11. Masood, M., Iqbal, S. (2024). Alkyl-phospholipid mediated cytotoxic and cytostatic effects in liver cancer cells. *Cancer Research and Medicine*, 1(2).

Uzunova, V.; Tzoneva, R.; Stoyanova, T.; Pankov, R.; Skrobanska, R.; Georgiev, G.; Maslenkova, L.; Tsonchev, Z.; Momchilova, A. (2019). Dimethylsphingosine and Miltefosine Induce Apoptosis in Lung Adenocarcinoma A549 Cells in a Synergistic Manner. Chem.-Biol. Interact., 310, 108731.

Citing Articles

1. Fu, F., Li, W., Zheng, X., Wu, Y., Du, D., Han, C. (2024). Role of Sphingosine-1-Phosphate Signaling Pathway in Pancreatic Diseases. *International Journal of Molecular Sciences*, 25(21), 11474.
2. El-Sheridy, N. A., El-Moslemany, R. M., Ramadan, A. A. (2021). Enhancing the in vitro and in vivo activity of itraconazole against breast cancer using miltefosine-modified lipid nanocapsules. *Drug Delivery*, 28(1), 906–919.
3. Latifi, A. (2020). Reviewing the effects of Miltefosine and suggesting it for the treatment of Coronavirus disease (COVID-19). *Infectious Diseases: Research and Treatment*, 13, 1178633720977488.
4. El-Sheridy, N. A., El-Moslemany, R. M., Ramadan, A. A. (2022). Itraconazole for topical treatment of skin carcinogenesis: Efficacy enhancement by lipid nanocapsule formulations. *Journal of Biomedical Nanotechnology*, 18(1), 97–111.
5. Zhang, C. Y., Hung, C. H., Hsiao, Y. L., Chang, T. M., Su, Y. C., Wang, L. C., Wang, S. M., Chen, S. H. (2024). Miltefosine reduces Coxsackievirus B3 lethality of mice with enhanced STAT3 activation. *Antiviral Research*, 223, 105824.
6. Fu, F., Li, W., Zheng, X., Wu, Y., Du, D., Han, C. (2024). Role of S1P Signaling Pathway in Pancreatic Diseases. *International Journal of Molecular Sciences*, 25(21), 11474.

Chapter 10. List of Participations in International and National Conferences

I. Presentation at a Scientific Event in the Country:

1. Membrane Phospholipids as Useful Target forAnti-Tumor Treatment with Erufosine, 3rd National Congress on Physical Sciences, Sofia, Bulgaria, Sep.9 – Oct.2, 2016.
2. Biomaterials Responding to Electrical Stimuli and Their Application in Tissue Engineering and Antitumor Therapy, Scientific Session "Biomedicine and Quality of Life – Young Researchers in Science," IBF-BMI-BAS, Sofia, Bulgaria, June 26–27, 2017.

II. Presentation at a Scientific Event Abroad or at an International Scientific Event in Our Country:

1. Study the effect of Erufosine on apoptosis and migration of cancer cells, YOUTH SCIENTIFIC CONFERENCE "KLIMENT'S DAYS", Sofia, Bulgaria, Nov. 16-17, 2017.
2. "EFFECT OF ERUFOSINE ON PROLIFERATION, INDUCTION OF APOPTOSIS AND MIGRATION OF MDA-MB-231 BREAST CANCER CELLS", Stoyanova T., Uzunova V., Popova D., Momchilova A., Berger M., Toshkova R. and Tzoneva R., VII National Conference with International Participation "Morphological Days", June 8 – 10, Sofia
3. „EFFECT OF ERUFOSINE AND SIMVASTATIN ON CELL PROLIFERATION AND MIGRATION IN BREAST CANCER CELLS MDA-MB 231 AND MCF-7", Stoyanova Tihomira,

Uzunova Veselina, Berger Martin, Momchilova Albena and Tzoneva Rumiana,Second scientific session “Biomedicine and quality of life”, November 4-5, 2019, Sofia.

4. “INVESTIGATION OF THE ANTI-CANCER EFFECT OF EXTRACTS FROM PETASITES HYBRIDUS L. (BUTTERBUR) ROOT ON BREAST CANCER CELL LINES” Tihomira Stoyanova, Veselina Uzunova, Albena Momchilova, Rumiana Tzoneva, Liliana Maslenkova, Scientific Conference “Kliment’s Days 2019”, November 8, 2019, Sofia.

Chapter 11. References

Bag, N., Huang, S., Wohland, T. (2015). Plasma membrane organization of epidermal growth factor receptor in resting and ligand-bound states. Biophysical Journal, 109(10), 1925–1936.

Birge, R. B., Boeltz, S., Kumar, S., Carlson, J., Wanderley, J., Calianese, D., Barcinski, Herrmann, M. (2016). Phosphatidylserine is a global immunosuppressive signal in efferocytosis, infectious disease, and cancer. Cell Death and Differentiation, 23(6), 962–978.

Bray, F. I., Laversanne, M., Weiderpass, E., & Soerjomataram, I. (2021). The ever-increasing importance of cancer as a leading cause of premature death worldwide. Cancer, 127(16), 3029–3030.

Casimiro, M. C., Crosariol, M., Loro, E., Li, Z., Pestell, R. G. (2012). Cyclins and cell cycle control in cancer and disease. Genes & Cancer, 3(11–12), 649–657.

Chometon, G., Cappuccini, F., Raducanu, A., Aumailley, M., Jendrossek, V. (2014). The membrane-targeted alkylphosphocholine erufosine interferes with survival signals from the extracellular matrix. Current Medicinal Chemistry, 21, 1747–1757.

Colombini, M. (2013). Membrane channels formed by ceramide. In Sphingolipids: Basic Science and Drug Development (pp. 109–126). Springer.

Dineva, I. K., Zaharieva, M. M., Konstantinov, S. M., Eibl, H., Berger, M. R. (2015). Erufosine suppresses breast cancer in vitro and in vivo for its activity on PI3K, c-Raf and Akt proteins. Breast Cancer Research and Treatment, 154, 591–604.

Georgieva, A., Toshkova, R., Uzunova, V., Berger, M. R., Tzoneva, R. (2015). In vivo antitumor effect of the novel alkylphosphocholine erufosine applied alone or in combination with doxorubicin against Graffi myeloid tumor in hamsters. In Biological Activity of Metals, Synthetic Compounds and Natural Products (74–81).

Herr, D. R., Chun, J. (2007). Effects of LPA and S1P on the nervous system and implications for their involvement in disease. Current Drug Targets, 8(1), 155–167.

Hilgard, P., Pohl, J., Engel, J. (1997). Alkylphosphocholines: A new class of membrane-active anticancer agents. Journal of Cancer Research and Clinical Oncology, 123(5), 286–287.

Hochegger, H., Takeda, S., Hunt, T. (2008). Cyclin-dependent kinases and cell-cycle transitions: Does one fit all? Nature Reviews Molecular Cell Biology, 9(11), 910–916.

Igarashi, Y., Kitamura, K., Toyokuni, T., et al. (1990). A specific enhancing effect of N,N-dimethylsphingosine on epidermal growth factor receptor autophosphorylation: Demonstration of its endogenous occurrence (and the virtual absence of unsubstituted sphingosine) in human epidermoid carcinoma A431 cells. Journal of Biological Chemistry, 265(10), 5385–5389.

Jiménez-López, J. M., Ríos-Marco, P., Marco, C., Segovia, J. L., Carrasco, M. P. (2010). Alterations in the homeostasis of phospholipids and cholesterol by antitumor alkylphospholipids. Lipids in Health and Disease, 9, 33.

Kapoor, V., Zaharieva, M. M., Das, S. N., Berger, M. R. (2012). Erufosine simultaneously induces apoptosis and autophagy by modulating the Akt–mTOR signaling pathway in oral squamous cell carcinoma. Cancer Letters, 319(1), 39–48.

Kuhlencord, A., Maniera, T., Eibl, H., Unger, C. (1992). Hexadecylphosphocholine: Oral treatment of visceral leishmaniasis in mice. Antimicrobial Agents and Chemotherapy, 36, 1630–1634.

Martelli, A. M., Papa, V., Tazzari, P. L., Ricci, F., Evangelisti, C., Chiarini, F., Mccubrey, J. A. (2010). Erucylphosphohomocholine, the first intravenously applicable alkylphosphocholine, is cytotoxic to acute myelogenous leukemia cells through JNK- and PP2A-dependent mechanisms. Leukemia, 24(4), 687–698.

McKay, T., Patel, M., Pickles, R. (2006). Influenza M2 envelope protein augments avian influenza hemagglutinin pseudotyping of lentiviral vectors. Gene Therapy, 13(9), 715–724.

Murad, H., Hawat, M., Ekhtiar, A., AlJapawe, A., Abbas, A., Darwish, H., Sbenati, O., Ghannam, A. (2016). Induction of G1-phase cell cycle arrest and apoptosis pathway in MDA-MB-231 human breast cancer cells by sulfated polysaccharide extracted from Laurencia papillosa. Cancer Cell International, 16, 39.

Nicoletti, I., Migliorati, G., Pagliacci, M. C., Grignani, F., Riccardi, C. (1991). A rapid and simple method for measuring thymocyte apoptosis by propidium iodide staining and flow cytometry. Journal of Immunological Methods, 139, 271–279.

Pachioni-Vasconcelos, J. A., Lopes, A. M., Apolinário, A. C., Valenzuela-Oses, J. K., Costa, J., Nascimento, L. O., Pessoa, A., Barbosa, L., Rangel-Yagui, C. O. (2016). Nanostructures for protein drug delivery. Biomaterials Science, 4, 205–218.

Park, S.-Y., Kim, J.-H., Choi, J.-H., Lee, C.-J., Lee, W.-J., Park, S., Park, Z.-Y., Baek, J.-H., Nam, J.-S. (2021). Lipid raft-disrupting miltefosine preferentially induces the death of colorectal cancer stem-like cells. Clinical and Translational Medicine, 11(11), e552.

Pehlivanova, V., Uzunova, V., Tsoneva, I., Berger, M. R., Ugrinova, I., Tzoneva, R. (2013). Effect of erufosine on the reorganization of cytoskeleton and cell death in adherent tumor and non-tumorigenic cells. Biotechnology & Biotechnological Equipment, 27(2), 3695–3699.

Scheiffele, P., Rietveld, A., Wilk, T., Simons, K. (1999). Influenza viruses select ordered lipid domains during budding from the plasma membrane. Journal of Biological Chemistry, 274(4), 2038–2044.

Shida, D., Takabe, K., Kapitonov, D., et al. (2008). Targeting SphK1 as a new strategy against cancer. Current Drug Targets, 9(8), 662–673.

Sigismund, S., Avanzato, D., Lanzetti, L. (2018). Emerging functions of the EGFR in cancer. Molecular Oncology, 12(1), 3–20.

Strub, G. M., Maceyka, M., Hait, N. C., Milstien, S., Spiegel, S. (2010). Extracellular and intracellular actions of sphingosine-1-phosphate. Advances in Experimental Medicine and Biology, 688, 141–155.

Sung, H., Ferlay, J., Siegel, R. L., Laversanne, M., Soerjomataram, I., Jemal, A., Bray, F. (2021). Global Cancer Statistics 2020: GLOBOCAN Estimates of Incidence and Mortality Worldwide for 36 Cancers in 185 Countries. CA: A Cancer Journal for Clinicians, 71(3), 209–249.

Takeda, M., Leser, G. P., Russell, C. J., Lamb, R. A. (2003). Influenza virus hemagglutinin concentrates in lipid raft microdomains for efficient viral fusion. Proceedings of the National Academy of Sciences of the USA, 100, 14610–14617.

Valenzuela-Oses, J. K., García, M. C., Feitosa, V. A., Pachioni-Vasconcelos, J. A., Gomes-Filho, S. M., Lourenço, F. R., Cerize, N. N. P., Bassères, D. S., Rangel-Yagui, C. O. (2017). Development and characterization of miltefosine-loaded polymeric micelles for cancer treatment. Materials Science and Engineering: C, 81, 327–333.

Vasconcelos, J. F., Meira, C. S., Silva, D. N., Nonaka, C. K. V., Daltro, P. S., Macambira, S. G., Domizi, P. D., Borges, V. M., Ribeiro-dos-Santos, R., de Freitas Souza, B. S., Soares, M. B. P. (2017). Therapeutic effects of sphingosine kinase inhibitor N,N-dimethylsphingosine (DMS) in experimental chronic Chagas disease cardiomyopathy. Scientific Reports, 7(1), 6171.

Yosifov, D., Todorov, P. T., Zaharieva, M. M., Georgiev, K. D., Pilicheva, B. A., Konstantinov, S. M., Berger, M. R. (2011). Erucylphospho-N,N,N- trimethylpropylammonium (erufosine) is a potential antimyeloma drug devoid of myelotoxicity. Cancer Chemotherapy and Pharmacology, 67(1), 13–25.

DECLARATION OF ORIGINALITY

(under Art. 27, para. 1 of the Law on the State of the Republic of Bulgaria on the Protection of Biological and Biological Resources)

As a doctoral student at the Institute of Biomedical Sciences of the Bulgarian Academy of Sciences, supervised by Prof. Dr Rumiana Tzoneva and Prof. Dr Albena Momchilova, D.sc.,

I DECLARE THAT:

1. The dissertation I am submitting for the defence for the degree of' doctor" on the topic "Antitumor lipids - influence on transmembrane cell signalling" is my original work and contains results obtained through scientific research conducted by me, with the support and/or assistance of my scientific supervisors;

2. The dissertation has not been previously submitted for the award of a scientific degree at any other higher education institution or scientific organisation;

3. I have adhered to copyright regulations concerning the sources I have used and have not unlawfully used texts from others without proper attribution of the author and source.